BornAgain

Software for simulating and fitting
X-ray and neutron small-angle scattering
at grazing incidence

User Manual

Version 1.3.0 (July 31, 2015)

Céline Durniak, Marina Ganeva, Gennady Pospelov,
Walter Van Herck, Joachim Wuttke

Scientific Computing Group
Jülich Centre for Neutron Science
at Heinz Maier-Leibnitz Zentrum Garching
Forschungszentrum Jülich GmbH

Homepage: http://www.bornagainproject.org

Copyright: Forschungszentrum Jülich GmbH 2013–2015

Licenses: Software: GNU General Public License version 3 or higher
Documentation: Creative Commons CC-BY-SA

Authors: Céline Durniak, Marina Ganeva, Gennady Pospelov,
Walter Van Herck, Joachim Wuttke
Scientific Computing Group
at Heinz Maier-Leibnitz Zentrum (MLZ) Garching

Disclaimer: Software and documentation are work in progress.
We cannot guarantee correctness and accuracy.
If in doubt, contact us for assistance or scientific collaboration.

Contents

Introduction **5**
About BornAgain . . . 5
About this Manual . . . 6
Typesetting conventions . . . 6

1 Online documentation **8**
1.1 Download and installation . . . 8
1.2 Further online information . . . 9
1.3 Registration, contact, discussion forum . . . 9

2 Small-angle scattering and the Born approximation **10**
2.1 Coherent neutron propagation . . . 10
2.2 Neutron scattering in Born approximation . . . 12
2.2.1 The Born expansion . . . 12
2.2.2 Far-field approximation . . . 13
2.2.3 Differential cross section . . . 15

3 Grazing-incidence scattering and the distorted wave Born approximation **16**
3.1 Scattering under grazing incidence . . . 16
3.1.1 Wave propagation in $2+1$ dimensions . . . 16
3.1.2 Distorted-wave Born approximation (DWBA) . . . 18
3.2 Absorption . . . 19

4 DWBA for multilayer systems **21**
4.1 Scalar case . . . 21
4.1.1 Wave propagation and DWBA matrix element . . . 21
4.1.2 Wave propagation across layers . . . 23
4.1.3 Damped waves in absorbing media or under total reflection . . . 26

5 Particle Assemblies **27**
5.1 Embedded particles . . . 27

A Some proofs **28**
A.1 Source–detector reciprocity for scalar waves . . . 28

B Form factor library **30**
B.1 AnisoPyramid (rectangle-based) . . . 34
B.2 Box (cuboid) . . . 36
B.3 Cone (circular) . . . 38
B.4 Cone6 (hexagonal) . . . 40
B.5 Cuboctahedron . . . 42
B.6 Cylinder . . . 44
B.7 EllipsoidalCylinder . . . 46
B.8 FullSphere . . . 48
B.9 HemiEllipsoid . . . 50
B.10 FullSpheroid . . . 52
B.11 Prism3 (triangular) . . . 54
B.12 Prism6 (hexagonal) . . . 56
B.13 Pyramid (square-based) . . . 58
B.14 Ripple1 (sinusoidal) . . . 60
B.15 Ripple2 (saw-tooth) . . . 62
B.16 Tetrahedron . . . 64
B.17 TruncatedCube . . . 66
B.18 TruncatedSphere . . . 70
B.19 TruncatedSpheroid . . . 72

Bibliography **74**

List of Symbols **75**

Index **78**

Introduction

About BornAgain

`BornAgain` is a software package to simulate and fit reflectometry, off-specular scattering, and grazing-incidence small-angle scattering (GISAS) of X-rays and neutrons. It provides a generic framework for modeling multilayer samples with smooth or rough interfaces and with various types of embedded nanoparticles. Support for neutron polarization and magnetic scattering is under development. The name, `BornAgain`, alludes to the central role of the distorted-wave Born approximation (DWBA) in the physical description of the scattering process.

`BornAgain` is being developed by the Scientific Computing Group of the Jülich Centre for Neutron Science (JCNS) at Heinz Maier-Leibnitz Zentrum (MLZ) Garching, Germany. It is intended to serve experimentalists in analysing all kinds of reflectometry data. It is equally aimed at users of MLZ reflectometers [1, 2, 3], at JCNS in-house researchers, and at the reflectometry and GISAS community at large. It is the main contribution of JCNS to national [4] and international [5] collaborations of large-scale facilities for the development of better user software.

`BornAgain` is released as free and open source software under the GNU General Public License (GPL, version 3 or higher). This documentation comes under the Creative Commons license CC-BY-SA.

The converse of this liberal policy is that we cannot guarantee correctness and accuracy of the code. It is entirely in the responsibility of users to convince themselves that their data interpretation is physically meaningful and plausible.

`BornAgain` is still under intense development. New major versions are released about every two months. When need arises, bugfix versions are released in between. It is strongly recommended that users regularly update their installations.

The software `BornAgain` embodies nontrivial scientific ideas. Therefore when `BornAgain` is used in preparing scientific papers, it is mandatory to cite the software:

> C. Durniak, M. Ganeva, G. Pospelov, W. Van Herck, J. Wuttke (2015),
> BornAgain — Software for simulating and fitting X-ray and neutron small-angle scattering at grazing incidence, version [...],
> http://www.bornagainproject.org

The initial design of BornAgain owes much to the widely used program IsGISAXS by Rémi Lazzari [6, 7]. Therefore when using BornAgain in scientific work, it might be appropriate to also cite the pioneering papers by Lazzari *et al.* [6, 8].

Since version 1.0, BornAgain almost completely reproduces the functionality of IsGISAXS. About 20 exemplary simulations have been tested against IsGISAXS, and found to agree up to almost the last floating-point digit. BornAgain goes beyond IsGISAXS in supporting an unrestricted number of layers and particles, diffuse reflection from rough layer interfaces and particles with inner structures. Support for neutron polarization and magnetic scattering is under development. Adhering to a strict object-oriented design, BornAgain provides a solid base for future extensions in response to specific user needs.

About this Manual

This user manual is complementary to the online documentation at http://www.bornagainproject.org. It does not duplicate information that is more conveniently read online. Therefore, Sect. 1 just contains a few pointers to the web site. The remainder of this manual mostly contains background on the scattering theory and on the sample models implemented in BornAgain, and some documentation of the corresponding Python functions.

This manual is incomplete. Several important chapters are still missing.

Specifically, we plan to provide documentation on

- X-ray propagation and scattering,
- polarized neutron propagation and magnetic scattering,
- mapping of $\partial\sigma/\partial\Omega$ onto flat detectors,
- scattering by rough interfaces,
- scattering by particle assemblies.

We intend to publish these chapters successively, along with new software release. To avoid confusion, starting with release 1.2 the manual carries the same version number as the software, even though it is in a less mature state.

We urge users to subscribe to our newsletter (see Sect. 1.3), and to contact us for any question not answered here or in the online documentation.

We are grateful for all kind of feedback: criticism, praise, bug reports, feature requests or contributed modules. If questions go beyond normal user support, we will be glad to discuss a scientific collaboration.

Typesetting conventions

In this manual, we use the following colored boxes to highlight certain information:

Such a box contains a **warning** about potential problems with the software or the documentation.

This road sign in the margin indicates **work in progress**.

Such a box contains an **implementation note** that explains how the theory exposed in this manual is actually used in `BornAgain`.

Such a box contains an **important fact**, for instance an equation that has a central role in the further development of the theory.

Variations of the equation sign (as $\equiv$, $:=$, $\doteq$) are explained in the symbol index, page 75. See there as well for less common mathematical functions like the cardinal sine function "sinc".

Chapter 1

Online documentation

This User Manual is complementary to the online documentation at the project web site http://www.bornagainproject.org. It does not duplicate information that is more conveniently read online. This brief chapter contains no more than a few pointers to the web site.

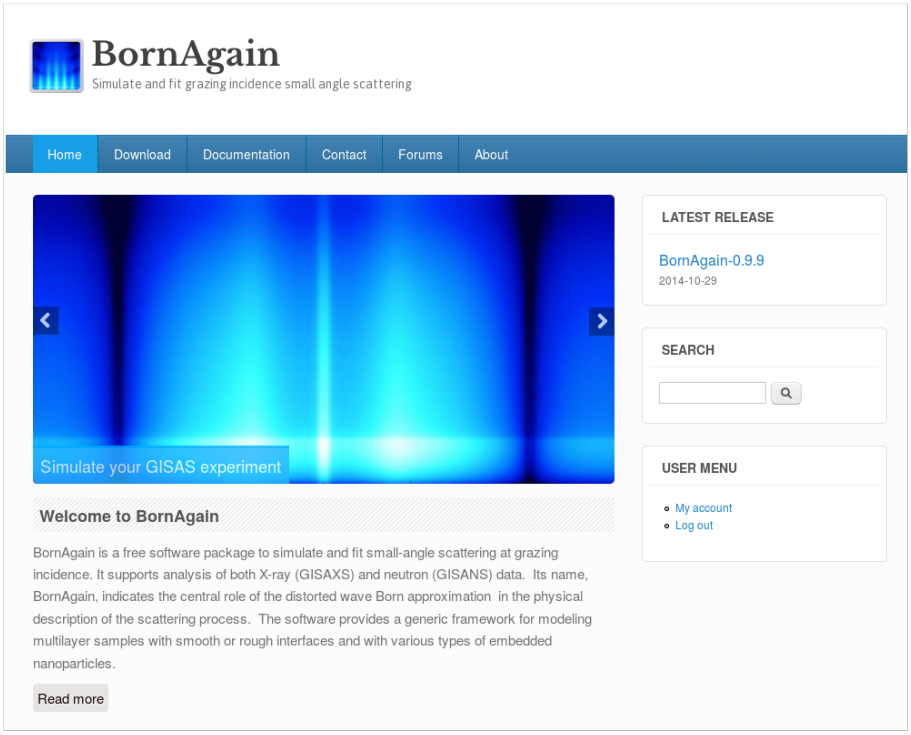
BornAgain
Simulate and fit grazing incidence small angle scattering
Home
Download
Documentation
Contact
Forums
About
Simulate your GISAS experiment
LATEST RELEASE
BornAgain-0.9.9
2014-10-29
SEARCH
USER MENU
My account
Log out
Welcome to BornAgain
BornAgain is a free software package to simulate and fit small-angle scattering at grazing incidence. It supports analysis of both X-ray (GISAXS) and neutron (GISANS) data. Its name, BornAgain, indicates the central role of the distorted wave Born approximation in the physical description of the scattering process. The software provides a generic framework for modeling multilayer samples with smooth or rough interfaces and with various types of embedded nanoparticles.
Read more

Figure 1.1: A screenshot of the home page http://www.bornagainproject.org.

1.1 Download and installation

`BornAgain` is a multi-platform software. We actively support the operating systems Linux, MacOS and Microsoft Windows. The DOWNLOAD section on the `BornAgain`

web site points to the download location for binary and source packages. It also provides a link to our `git` server where the unstable development trunk is available for contributors or for users who want to live on the edge.

The DOCUMENTATION section contains pages with *Installation instructions*.

1.2 Further online information

The DOCUMENTATION section of the project web site contains in particular

- an overview of the software architecture,
- a list of implemented functionality,
- tutorials for "Working with `BornAgain`", using either the Graphical User Interface or `Python` scripts,
- a comprehensive collection of examples that demonstrate how to use `BornAgain` for modeling various sample structures and different experimental conditions,
- a link to the API reference for using `BornAgain` through `Python` scripts or C++ programs.

1.3 Registration, contact, discussion forum

To stay informed about the ongoing development of `BornAgain`, register on the project homepage `http://www.bornagainproject.org` ("Create new account"). You will then receive our occasional newsletters, and be authorized to post to the discussion forum.

To contact the `BornAgain` development and maintenance team in the Scientific Computing Group of Heinz Maier-Leibnitz Zentrum (MLZ) Garching, write a mail to `contact@bornagainproject.org`, or fill the form in the CONTACT section of the project web site.

For questions that might be of wider interest, please consider posting to the discussion forum, accessible through the FORUMS tab of the project web site.

Chapter 2

Small-angle scattering and the Born approximation

This chapter introduces the basic theory of small-angle scattering (SAS). We specifically consider scalar neutron propagation, adjourning the notationally more involved vectorial theory of X-rays and polarized neutrons a later edition. Our exposition is self-contained, except for the initial passage from the microscopic to the macroscopic Schrödinger equation, which we outline only briefly (Sect. 2.1). The standard description of scattering in first order Born approximation is introduced in a way that is suitable subsequent modification into the distorted wave Born approximation needed for grazing-incidence small-angle scattering (Sect.2.2).

2.1 Coherent neutron propagation

The scalar wavefunction $\psi(\boldsymbol{r}, t)$ of a free neutron is governed by the microscopic Schrödinger equation

$$i\hbar\partial_t\psi(\boldsymbol{r}, t) = \left\{-\frac{\hbar^2}{2m}\boldsymbol{\nabla}^2 + V(\boldsymbol{r})\right\}\psi(\boldsymbol{r}, t). \tag{2.1}$$

By assuming a time-independent potential $V(\boldsymbol{r})$, we have excluded inelastic scattering. Therefore we only need to consider monochromatic waves with given frequency ω. In consequence, we have a stationary wavefunction

$$\psi(\boldsymbol{r}, t) = \psi(\boldsymbol{r})\mathrm{e}^{-i\omega t}. \tag{2.2}$$

The minus sign in the exponent of the phase factor is an inevitable consequence of the standard form of the Schrödinger equation, and is therefore called the *quantum-mechanical sign convention*. For electromagnetic radiation usage is less uniform. While most optics textbooks have adopted the quantum-mechanical convention (2.2), in X-ray crystallography the conjugate phase factor $\mathrm{e}^{+i\omega t}$ is prefered. This *crystallographic sign convention* has also been chosen in influential texts on GISAXS (e.g. [8]). Here, however, we are concerned not only with X-rays, but also with neutrons, and therefore we need to leave the Schrödinger equation (2.1) intact. Thence:

In this manual, and in the program code of `BornAgain`, the quantum-mechanical sign convention (2.2) is chosen. This has implications for the sign of the imaginary part of the refractive index, as explained in Sect. 3.2.

Inserting (2.2) in (2.1), we obtain the stationary Schrödinger equation

$$\left\{-\frac{\hbar^2}{2m}\boldsymbol{\nabla}^2 + V(\boldsymbol{r}) - \hbar\omega\right\}\psi(\boldsymbol{r}) = 0. \tag{2.3}$$

The *nuclear* (or *microscopic*) *optical potential* $V(\boldsymbol{r})$, in a somewhat "naive conception" [9, p. 7], consists of a sum of delta functions, representing Fermi's "pseudopotential". The superposition of the incident wave with the scattered waves originating from each illuminated nucleus results in *coherent forward scattering*, in line with Huygens' principle.

Coherent superposition also leads to *Bragg scattering*. However, Bragg scattering by atomic lattices only occurs at angles far above the small-angle range covered in GISAS experiments. Accordingly, it can be neglected in the analysis of GISAS data, or at most, is taken into account as a loss channel.

Therefore, we can neglect the atomic structure of $V(\boldsymbol{r})$, and perform some coarse graining to arrive at a *continuum approximation*. This is similar to the passage from the microscopic to the macroscopic Maxwell equations. The details are intricate [9, 10], but the result [9, eq. 2.8.32] looks very simple: The macroscopic field equation has still the form of a stationary Schrödinger equation,

$$\left\{-\frac{\hbar^2}{2m}\boldsymbol{\nabla}^2 + v(\boldsymbol{r}) - \hbar\omega\right\}\psi(\boldsymbol{r}) = 0, \tag{2.4}$$

where ψ now stands for the *coherent wavefunction* obtained by superposition of incident and forward scattered states, and $v(\boldsymbol{r})$ is the *macroscopic optical potential*. This potential is weak, and slowly varying compared to atomic length scales. It can be rewritten in a number of ways, especially in terms of a *bound scattering length density* $\rho_s(\boldsymbol{r})$ [9, eq. 2.8.37],

$$v(\boldsymbol{r}) = \frac{2\pi\hbar^2}{m}\rho_s(\boldsymbol{r}), \tag{2.5}$$

or of a *refractive index* $n(\boldsymbol{r})$ defined by

$$n(\boldsymbol{r})^2 := 1 - \frac{4\pi}{K^2}\rho_s(\boldsymbol{r}) = 1 - \frac{2m}{\hbar^2K^2}v(\boldsymbol{r}). \tag{2.6}$$

In the latter expression, we introduced the *vacuum wavenumber* K, which is connected with the frequency ω through the *dispersion relation*

$$\frac{\hbar^2K^2}{2m} = \hbar\omega. \tag{2.7}$$

Since we only consider stationary solutions (2.2), ω will not appear any further in our derivations. Instead, we use K as the given parameter that characterizes the incoming radiation. In terms of K and n, the macroscopic Schrödinger equation (2.4) can be rewritten as

$$\left\{\boldsymbol{\nabla}^2 + K^2 n(\boldsymbol{r})^2\right\}\psi(\boldsymbol{r}) = 0. \tag{2.8}$$

This equation is the starting point for the analysis of all small-angle scattering experiments, whether under grazing incidence (GISAS) or not (regular SAS).

2.2 Neutron scattering in Born approximation

2.2.1 The Born expansion

To describe an elastic scattering experiment, we need to solve the Schrödinger equation (2.8) under the asymptotic boundary condition

$$\psi(\boldsymbol{r}) \simeq \psi_\mathrm{i}(\boldsymbol{r}) + f(\vartheta,\varphi)\frac{\mathrm{e}^{iKr}}{4\pi r} \text{ for } r \to \infty, \tag{2.9}$$

where $\psi_\mathrm{i}(\boldsymbol{r})$ is the incident wave as prepared by the experimental apparatus, and the second term on the right-hand side is the outgoing scattered wave that carries information in form of the angular distribution $f(\vartheta,\varphi)$.

For thermal or cold neutrons, as for X-rays, the refractive index n is almost always very close to 1. This suggests a solution of the Schrödinger equation by means of a perturbation expansion in powers of $n^2 - 1$. This expansion is named after Max Born who introduced it in quantum mechanics.[1]

To carry out this idea, we rewrite the Schrödinger equation once more so that it takes the form of a Helmholtz equation with a perturbation term on the right side:

$$\left(\boldsymbol{\nabla}^2 + K^2\right)\psi(\boldsymbol{r}) = 4\pi\chi(\boldsymbol{r})\psi(\boldsymbol{r}) \tag{2.10}$$

with

$$\chi(\boldsymbol{r}) := \frac{K^2}{4\pi}\left(1 - n^2(\boldsymbol{r})\right). \tag{2.11}$$

This definition just compensates (2.6) so that $\chi = \rho_s$. In the following, we prefer the notation χ and the appellation *perturbative potential* over the scattering length density ρ_s to prepare for the generalization to the electromagnetic case.

Equation (2.10) looks like an inhomogeneous differential equation — provided we neglect for a moment that the unknown function ψ reappears on the right side. The homogeneous equation

$$\left(\boldsymbol{\nabla}^2 + K^2\right)\psi(\boldsymbol{r}) = 0 \tag{2.12}$$

is solved by plane waves and superpositions thereof. It applies in particular to the incident wave ψ_i.

[1] It goes back to Lord Rayleigh who devised it for sound, and later also applied it to electromagnetic waves, which resulted in his famous explanation of the blue sky.

For an isolated inhomogeneity,

$$(\boldsymbol{\nabla}^2 + K^2)\, G(\boldsymbol{r}, \boldsymbol{r}') = \delta(\boldsymbol{r} - \boldsymbol{r}') \tag{2.13}$$

is solved by the Green function[2]

$$G(\boldsymbol{r}, \boldsymbol{r}') = \frac{\mathrm{e}^{iK|\boldsymbol{r}-\boldsymbol{r}'|}}{4\pi|\boldsymbol{r} - \boldsymbol{r}'|}, \tag{2.14}$$

which is an outgoing spherical wave centered at $\boldsymbol{r}'$. Convoluting this function with the given inhomogeneity $4\pi\chi\psi$, we obtain what is known as the Lippmann-Schwinger equation,

$$\psi(\boldsymbol{r}) = \psi_\mathrm{i}(\boldsymbol{r}) + \int \mathrm{d}^3 r'\, G(\boldsymbol{r}, \boldsymbol{r}') 4\pi\chi(\boldsymbol{r}')\psi(\boldsymbol{r}'). \tag{2.15}$$

This integral equation for $\psi(\boldsymbol{r})$ improves upon the original stationary Schrödinger equation (2.10) in that it ensures the boundary condition (2.9). It can be resolved into an infinite series by iteratively substituting the full right-hand side of (2.15) into the integrand. Successive terms in this series contain rising powers of χ. Since χ is assumed to be small, the series is likely to converge. In *first-order Born approximation*, only the linear order in χ is retained,

$$\psi(\boldsymbol{r}) \doteq \psi_\mathrm{i}(\boldsymbol{r}) + 4\pi \int \mathrm{d}^3 r'\, G(\boldsymbol{r}, \boldsymbol{r}')\chi(\boldsymbol{r}')\psi_\mathrm{i}(\boldsymbol{r}'). \tag{2.16}$$

This is practically always adequate for material investigations with X-rays or neutrons, where the aim is to deduce $\chi(\boldsymbol{r}')$ from the scattered intensity $|\psi(\boldsymbol{r})|^2$. Since detectors are always placed at positions $\boldsymbol{r}$ that are not illuminated by the incident beam, we are only interested in the scattered wave field

$$\psi_\mathrm{s}(\boldsymbol{r}) := 4\pi \int \mathrm{d}^3 r'\, G(\boldsymbol{r}, \boldsymbol{r}')\chi(\boldsymbol{r}')\psi_\mathrm{i}(\boldsymbol{r}'). \tag{2.17}$$

2.2.2 Far-field approximation

We can further simplify (2.17) under the conditions of Fraunhofer diffraction: the distance from the sample to the detector location $\boldsymbol{r}$ must be much larger than the size of the sample. Since the scattered wave $\psi_\mathrm{s}(\boldsymbol{r})$ only depends on $\boldsymbol{r}$ through the Green function $G(\boldsymbol{r}, \boldsymbol{r}')$, we shall derive a far-field approximation for the latter.

We choose the origin within the sample so that the integral in (2.17) runs over $\boldsymbol{r}'$ with $r' \ll r$. This allows us to expand

$$\left|\boldsymbol{r} - \boldsymbol{r}'\right| \doteq \sqrt{r^2 - 2\boldsymbol{r}\,\boldsymbol{r}'} \doteq r - \frac{\boldsymbol{r}\,\boldsymbol{r}'}{r} \equiv r - \frac{\boldsymbol{k}_\mathrm{f}\boldsymbol{r}'}{K}, \tag{2.18}$$

[2]Verification under the condition $\boldsymbol{r} \neq 0$ is a straightforward exercise in vector analysis. For the special case $\boldsymbol{r} = 0$, one encloses the origin in a small sphere and integrates by means of the Gauss-Ostrogadsky divergence theorem. This explains the appearance of the factor 4π.

where we have introduced the outgoing wavevector

$$\boldsymbol{k}_\mathrm{f} := K\frac{\boldsymbol{r}}{r}. \tag{2.19}$$

We apply this to (2.14), and obtain in leading order the far-field Green function

$$G_\mathrm{far}(\boldsymbol{r},\boldsymbol{r'}) = \frac{\mathrm{e}^{iKr}}{4\pi r}\psi_\mathrm{f}^*(\boldsymbol{r'}) \tag{2.20}$$

where

$$\psi_\mathrm{f}(\boldsymbol{r}) := \mathrm{e}^{i\boldsymbol{k}_\mathrm{f}\boldsymbol{r}} \tag{2.21}$$

is a plane wave propagating towards the detector, and ψ^* designates the complex conjugate of ψ. With respect to $\boldsymbol{r}$, G_far is an outgoing spherical wave.

The scattered wave (2.17) becomes in the far-field approximation

$$\psi_\mathrm{s,far}(\boldsymbol{r}) = \frac{\mathrm{e}^{iKr}}{r}\langle\psi_\mathrm{f}|\chi|\psi_\mathrm{i}\rangle\,, \tag{2.22}$$

where we used Dirac notation for the transition matrix element

$$\langle\psi_\mathrm{f}|\chi|\psi_\mathrm{i}\rangle := \int \mathrm{d}^3r\,\psi_\mathrm{f}^*(\boldsymbol{r})\chi(\boldsymbol{r})\psi_\mathrm{i}(\boldsymbol{r}). \tag{2.23}$$

In order to reconcile conflicting sign conventions, we will in the following rather use its complex conjugate $\langle\psi_\mathrm{i}|\chi|\psi_\mathrm{f}\rangle = \langle\psi_\mathrm{f}|\chi|\psi_\mathrm{i}\rangle^*$. Under the standard assumption that the incident radiation is a plane wave

$$\psi_\mathrm{i}(\boldsymbol{r}) = \mathrm{e}^{i\boldsymbol{k}_\mathrm{i}\boldsymbol{r}} \tag{2.24}$$

with $k_\mathrm{i} = K$, the matrix element takes the form

$$\langle\psi_\mathrm{i}|\chi|\psi_\mathrm{f}\rangle = \int \mathrm{d}^3r\,e^{-i\boldsymbol{k}_\mathrm{i}\boldsymbol{r}}\chi(\boldsymbol{r})e^{i\boldsymbol{k}_\mathrm{f}\boldsymbol{r}} = \int \mathrm{d}^3r\,e^{i\boldsymbol{q}\boldsymbol{r}}\chi(\boldsymbol{r}) =: \chi(\boldsymbol{q}), \tag{2.25}$$

where we have introduced the *scattering vector*[3]

$$\boldsymbol{q} := \boldsymbol{k}_\mathrm{f} - \boldsymbol{k}_\mathrm{i} \tag{2.26}$$

and the notation $\chi(\boldsymbol{q})$ for the Fourier transform of the perturbative potential, which is what small-angle neutron scattering basically measures.

[3]With this choice of sign, $\hbar\boldsymbol{q}$ is the momentum *gained* by the scattered neutron, and *lost* by the sample. In much of the literature the opposite convention is prefered, since it emphasizes the sample physics over the scattering experiment. However, when working with twodimensional detectors it is highly desirable to express pixel coordinates and scattering vector components with respect to equally oriented coordinate axes, which can only be achieved by the convention (2.26).

2.2.3 Differential cross section

In connection with (2.16) we mentioned that a scattering experiment measures intensities $|\psi(\boldsymbol{r})|^2$. We shall now restate this in a more rigorous way. In the case of neutron scattering, one actually measures a *probability flux*. We define it in arbitrary relative units as

$$\boldsymbol{J}(\boldsymbol{r}) := \psi^* \frac{\boldsymbol{\nabla}}{2i}\psi - \psi \frac{\boldsymbol{\nabla}}{2i}\psi^*. \tag{2.27}$$

The ratio of the scattered flux hitting an infinitesimal detector area $r^2 \mathrm{d}\Omega$ to the incident flux is expressed as a *differential cross section*

$$\frac{\mathrm{d}\sigma}{\mathrm{d}\Omega} := \frac{r^2 J(\boldsymbol{r})}{J_\mathrm{i}}. \tag{2.28}$$

With (2.24), the incident flux is

$$\boldsymbol{J}_\mathrm{i} = \boldsymbol{k}_\mathrm{i}. \tag{2.29}$$

With (2.22), the scattered flux at the detector is

$$\boldsymbol{J}(\boldsymbol{r}) = \hat{\boldsymbol{r}} \frac{K}{r^2} |\langle \psi_\mathrm{i} | \chi | \psi_\mathrm{f} \rangle|^2. \tag{2.30}$$

From (2.28) we obtain the generic differential cross section of elastic scattering in first order Born approximation,

$$\frac{\mathrm{d}\sigma}{\mathrm{d}\Omega} = |\langle \psi_\mathrm{i} | \chi | \psi_\mathrm{f} \rangle|^2. \tag{2.31}$$

As we shall see below, it holds not only for plane waves governed by the vacuum Helmholtz equation (2.12), but also for distorted waves.

In the plane-wave case (2.25) considered here, the differential cross section is just the squared modulus of the Fourier transform of the perturbative potential,

$$\frac{\mathrm{d}\sigma}{\mathrm{d}\Omega} = |\chi(\boldsymbol{q})|^2. \tag{2.32}$$

Chapter 3

Grazing-incidence scattering and the distorted wave Born approximation

In this chapter, introduce grazing-incidence small-angle scattering and its standard theoretical treatment by means of the distorted wave Born approximation (Sect. 3.1). We also discuss the treatment of absorption (Sect. 3.2).

3.1 Scattering under grazing incidence

3.1.1 Wave propagation in $2+1$ dimensions

Reflectometry and grazing-incidence scattering are designed for the investigation of surfaces, interfaces, and thin layers, or most generically: samples with a $2+1$ dimensional structure that are on average translationally invariant in x and y direction, but structured in z direction. By convention, we designate the *sample plane* (xy) as *horizontal*, and the *sample normal* (z) as *vertical*, even if this does not correspond to the actual experimental geometry.[1] The z axis points upwards, hence out of the sample towards the vacuum (or air) halfspace where the incident radiation comes from, as illustrated in Fig. 3.1.

Vertical modulations of the refractive index $n(\boldsymbol{r})$ cause refraction and reflection of an incident plane wave. For small glancing angles, these distortions can be arbitrary large, up to the limiting case of total reflection, even though $1-n$ is only of the order 10^{-5} or smaller. Such zeroth-order effects cannot be accounted for by perturbative scattering theory. Instead, we need to deal with refraction and reflection at the level of the wave propagation equation. We move the vertical variations of the squared refractive index to the left-hand side of the Schrödinger equation (2.8),

$$\left\{\boldsymbol{\nabla}^2 + K^2\overline{n^2}(z)\right\}\psi(\boldsymbol{r}) = 4\pi\chi(\boldsymbol{r})\psi(\boldsymbol{r}), \tag{3.1}$$

where the overline indicates an horizontal average. Deviating from (2.11), the perturbation has been redefined as

$$\chi(\boldsymbol{r}) := \frac{K^2}{4\pi}\left(\overline{n^2}(z) - n^2(\boldsymbol{r})\right), \tag{3.2}$$

[1] In many reflectometers, the scattering plane and the sample normal are horizontal in laboratory space.

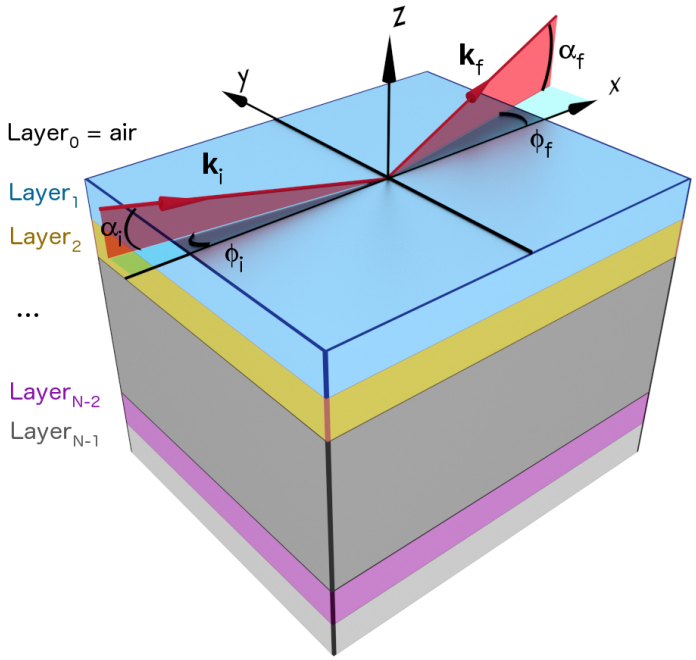

Figure 3.1: Geometric conventions in GISAS scattering comprise a Cartesian coordinate system and a set of angles. The coordinate system has a z axis normal to the sample plane, and pointing into the halfspace where the beam comes from. The x axis usually points along the incident beam, projected onto the sample plane. Incident and final plane waves are characterized by wavevectors $\boldsymbol{k}_\mathrm{i}$, $\boldsymbol{k}_\mathrm{f}$; the angle α_i is the incident glancing angle; ϕ_i is usually zero, unless used to describe a sample rotation; α_f is the exit angle with respect to the sample's surface; and ϕ_f is the scattering angle with respect to the scattering plane. The numbered layers illustrate a multilayer system as dicussed in Sect. 4.

which only accounts for horizontal fluctuations of the refractive index. Wave propagation, unperturbed by χ, but including refraction and reflection effects, obeys the homogeneous equation

$$\left\{\boldsymbol{\nabla}^2 + K^2\overline{n^2}(z)\right\}\psi(\boldsymbol{r}) = 0. \tag{3.3}$$

It is solved for the horizontal coordinate $\boldsymbol{r}_\parallel$ by the factorization ansatz

$$\psi(\boldsymbol{r}) = \mathrm{e}^{i\boldsymbol{k}_\parallel \boldsymbol{r}_\parallel}\phi(z). \tag{3.4}$$

The horizontal wavevector $\boldsymbol{k}_\parallel$ remains constant as initialized by the incoming beam. The vertical wavefunction must fulfill

$$\left\{\partial_z^2 + K^2\overline{n^2}(z) - k_\parallel^2\right\}\phi(z) = 0. \tag{3.5}$$

When an incident plane wave, travelling downwards with $\phi(z) = \mathrm{e}^{-ik_\perp z}$, impinges on a sample with $\overline{n^2}(z) \neq 1$, then the wave is partly reflected ($-k_\perp$ reversed into

$+k_\perp$) and partly refracted ($k_\perp$ changing while $\boldsymbol{k}_\parallel$ stays constant, resulting in a change of glancing angle). Similarly, reflection and refraction occur whenever $\overline{n^2}(z)$ varies within the sample. As a result, at any z within the zone where $\overline{n^2}(z)$ varies, the vertical wavefunction $\phi(z)$ is composed of a downward travelling component $\phi^-(z)$ and an upward travelling component $\phi^+(z)$.

For a graded refractive index $\overline{n^2}$ that is a smooth function of z, the differential equation (3.5) is best solved using the WKB method.[2] If otherwise $\overline{n^2}(z)$ is discontinuous at some interface $z = z_j$, then the limiting values of $\phi^-(z)$ and $\phi^+(z)$ on approaching z_j from above or below are connected to each other through Fresnel's transmission and reflection coefficients. This applies in particular to multilayer systems, discussed in chapter 4.

3.1.2 Distorted-wave Born approximation (DWBA)

The standard form of the Born approximation, as presented in Sect. 2.2, combines an approximation scheme (computing (2.15) by iteration) with an assumption (the incident field is a plane wave) and an analytic result (in far-field approximation, the Green function of the Helmholtz equation is a plane wave with respect to the locus of scattering). These three elements must not necessarily go together. We can apply the very same approximation scheme, even if the incident field is not a plane wave, but a *distorted wave*, namely a superposition of downwards and upwards travelling plane waves, as derived in the previous section. This is the core idea of the *distorted-wave Born approximation* (DWBA).[3]

To carry out this idea, we need to determine the Green function G. In Sect. 2.2.1 we did so quite specifically for a homogeneous material. Computing G in closed form for a more generic wave equation like (3.3) is far more difficult, if not outright impossible. Fortunately, this computation is not necessary, and would be but wasted effort: We do not need the full solution $G(\boldsymbol{r}, \boldsymbol{r}')$, but only its asymptotic far-field value $G(\boldsymbol{r}_\mathrm{D}, \boldsymbol{r}')$ at a detector position $\boldsymbol{r}_\mathrm{D}$. Thanks to a *source-detector reciprocity theorem* (A.10) proven in Appendix A.1, we can compute this value as

$$G(\boldsymbol{r}_\mathrm{D}, \boldsymbol{r}) = B(\boldsymbol{r}, \boldsymbol{r}_\mathrm{D}), \tag{3.6}$$

where B is the *adjoint Green function* that describes backward propagation from $\boldsymbol{r}_\mathrm{D}$ into the sample.

Outside the sample, B obeys the Helmholtz equation with isolated inhomogeneity (2.13), and therefore has the far-field expansion (2.20),

$$B_\mathrm{far}(\boldsymbol{r}, \boldsymbol{r}_\mathrm{D}) = \frac{\mathrm{e}^{iKr_\mathrm{D}}}{4\pi r_\mathrm{D}} \mathrm{e}^{-i\boldsymbol{k}_\mathrm{f}\boldsymbol{r}}. \tag{3.7}$$

When this backward propagating plane waves impinges on the sample, it undergoes reflection and refraction in exactly the same way as the incident plane wave $\mathrm{e}^{i\boldsymbol{k}_\mathrm{i}\boldsymbol{r}}$.

[2] Also called *semiclassical approximation* or *phase integral method*, named after Wentzel (1926), Kramers (1926), Brillouin (1926). See any textbook on quantum mechanics.

[3] The distorted-wave Born approximation was originally devised by Massey and Mott (ca 1933) for collisions of charged particles.

Therefore, (3.7) admits a generalization that also holds inside the sample:

$$B_{\text{far}}(\boldsymbol{r}, \boldsymbol{r}_{\text{D}}) = \frac{\mathrm{e}^{iKr_{\text{D}}}}{4\pi r_{\text{D}}} \psi_{\text{f}}^*(\boldsymbol{r}). \tag{3.8}$$

Applying now the reciprocity theorem (3.6), we obtain

$$G_{\text{far}}(\boldsymbol{r}, \boldsymbol{r}') = \frac{\mathrm{e}^{iKr}}{4\pi r} \psi_{\text{f}}^*(\boldsymbol{r}') \tag{3.9}$$

which agrees literally with (2.20), though ψ_{f} is not any longer a plane wave. Accordingly, the scattered far-field is still given by (2.22), and the differential cross section by (2.31). We only need to redetermine the matrix element $\langle\psi_{\text{i}}|\chi|\psi_{\text{f}}\rangle$, which no longer has the plane-wave form (2.25).

Since both the incident and the scattered distorted wavefunction are composed of downward and upward propagating waves,

$$\psi_w(\boldsymbol{r}) = \psi_w^-(\boldsymbol{r}) + \psi_w^+(\boldsymbol{r}) \quad \text{with} \quad w = \text{i}, \text{f}, \tag{3.10}$$

the matrix element can be expanded into four terms,

$$\langle\psi_{\text{i}}|\chi|\psi_{\text{f}}\rangle = \langle\psi_{\text{i}}^-|\chi|\psi_{\text{f}}^-\rangle + \langle\psi_{\text{i}}^-|\chi|\psi_{\text{f}}^+\rangle + \langle\psi_{\text{i}}^+|\chi|\psi_{\text{f}}^-\rangle + \langle\psi_{\text{i}}^+|\chi|\psi_{\text{f}}^+\rangle\,, \tag{3.11}$$

or in an obvious shorthand notation

$$\langle\psi_{\text{i}}|\chi|\psi_{\text{f}}\rangle = \sum_{\pm_{\text{i}}} \sum_{\pm_{\text{f}}} \langle\psi_{\text{i}}^{\pm}|\chi|\psi_{\text{f}}^{\pm}\rangle\,. \tag{3.12}$$

This equation contains the essence of the distorted-wave Born approximation for small-angle scattering under grazing incidence, and is the base for all scattering models implemented in `BornAgain`. Since $\langle\psi_{\text{i}}|\chi|\psi_{\text{f}}\rangle$ appears as a squared modulus in the differential cross section (2.31), the four terms of (3.12) can interfere with each other, which adds to the complexity of GISAS patterns.

3.2 Absorption

The complex refractive index of a given material shall be written as

$$n \doteq 1 - \delta + i\beta, \tag{3.13}$$

introducing two small real parameters δ, β. However, in our derivations, which are all rooted in (2.8), n only appears as n^2. Therefore, we actually *define*

$$n^2 := 1 - 2\delta + 2i\beta, \tag{3.14}$$

and read (3.13) as an excellent approximation.

While the real part of n is responsible for refraction, reflection, and scattering, the imaginary part describes absorption and leads to a damping of propagating waves. The

plus sign in front of the imaginary part is a consequence of the quantum-mechanical sign convention; in the X-ray crystallography convention it would be a minus sign.

The factorization ansatz (3.4) leaves us some freedom how to deal with an imaginary part of n. We *choose* that horizontal wavevectors $\boldsymbol{k}_\parallel$ shall always be real. The damping then appears in the vertical wavefunction $\phi(z)$ that is governed by the complex wave equation (3.5).

Chapter 4

DWBA for multilayer systems

In Sect. 3.1, we have discussed wave propagation and scattering in 2+1 dimensional systems that are translationally invariant in the horizontal xy plane, and have a vertical refractive index profile $\overline{n^2}(z)$. Here we specialize to layered systems where $\overline{n^2}(z)$ is a step function that is constant within one layer. First, only scalar interactions are considered. Later, the theory is extended to account for polarization effects.

By convention, layers are numbered from top to bottom (see Fig. 4.1). The top vacuum (or air) layer (which extends to $z \to +\infty$) has number 0, the substrate (extending to $z \to -\infty$) is layer N.

All layer interfaces are assumed to be perfectly smooth. Support for rough interfaces is already implemented in `BornAgain`, but documentation is adjourned to a later edition of this manual.

4.1 Scalar case

4.1.1 Wave propagation and DWBA matrix element

To compute scattering cross sections in DWBA, we first need to determine the distorted wavefunctions $\psi_w(\boldsymbol{r})$ for $\boldsymbol{r}$ inside the sample. The following derivation holds for the incoming wave ($w = \mathrm{i}$) as well as for the back-traced detected wave ($w = \mathrm{f}$).

We consider wave propagation in one layer l with constant average refractive index $\overline{n^2}(z) = \overline{n_l^2}$. A vacuum plane wave, impinging on a layered structure, is at each interface partly reflected, partly refracted, so that the wavefunction inside a material layer has an upward and a downward propagating component, as per (3.10). Each component is a plane wave, with a wavevector

$$\boldsymbol{k}_{wl}^{\pm} = \boldsymbol{k}_{\parallel w} \pm k_{\perp wl}\hat{\boldsymbol{z}}. \tag{4.1}$$

As explained in connection with (3.4), the in-plane wavevector $\boldsymbol{k}_{\parallel w}$ remains constant across layer interfaces. The vertical wavenumber is obtained from (3.5),

$$k_{\perp wl} = \sqrt{K^2\overline{n_l^2} - k_{\parallel w}^2}. \tag{4.2}$$

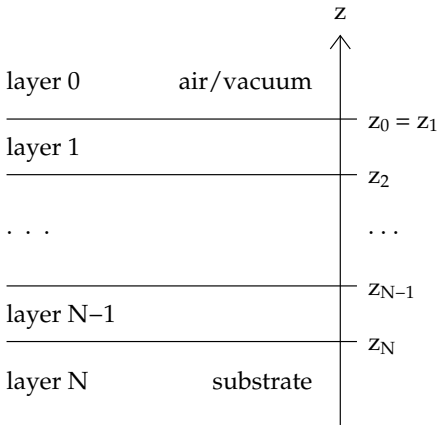

Figure 4.1: The parameter z_l is the z coordinate of the *top* interface of layer l, except for z_0 which is the coordinate of the *bottom* interface of the air/vacuum layer 0.

We factorize the corresponding wavefunctions as

$$\psi^{\pm}_{wl}(\boldsymbol{r}) = \mathrm{e}^{i\boldsymbol{k}_{\parallel w}\boldsymbol{r}_{\parallel}}\phi^{\pm}_{wl}(z), \tag{4.3}$$

with vertical propagation described by a one-dimensional wavefunction

$$\phi^{\pm}_{wl}(z) = A^{\pm}_{wl}\mathrm{e}^{\pm i k_{\perp wl}(z-z_l)}. \tag{4.4}$$

For later convenience, the phase factor in (4.4) includes an offset z_l as defined in Fig. 4.1. The amplitudes A are often written with distinct letters T and R to designate the transmitted or reflected beam,

$$T_{wl} \coloneqq A^{-}_{wl}, \quad R_{wl} \coloneqq A^{+}_{wl}. \tag{4.5}$$

They need to be computed recursively, as described in the following subsection 4.1.2.

In the absence of absorption, wavevectors are real so that we can describe the beam in terms of a glancing angle

$$\alpha_{wl} \coloneqq \arctan(k_{\perp wl}/k_{\parallel w}). \tag{4.6}$$

Equivalently,

$$k_{\parallel w} = K n_l \cos\alpha_{wl}. \tag{4.7}$$

Since $k_{\parallel w}$ is constant across layers, we have

$$n_l \cos\alpha_{wl} = \text{the same for all } l, \tag{4.8}$$

which is Snell's refraction law.

Since the $\psi^{\pm}_{wl}$ are plane waves within layer l, we can at once write down the DWBA transition matrix element (3.12)

$$\langle\psi_{\mathrm{i}}|\chi|\psi_{\mathrm{f}}\rangle = \sum_l \sum_{\pm_{\mathrm{i}}} \sum_{\pm_{\mathrm{f}}} A^{\pm *}_{\mathrm{i}l} A^{\pm}_{\mathrm{f}l} \chi_l(\boldsymbol{k}^{\pm}_{\mathrm{f}l} - \boldsymbol{k}^{\pm}_{\mathrm{i}l}), \tag{4.9}$$

where

$$\chi_l(\boldsymbol{q}) \coloneqq \int_{z_l}^{z_{l-1}} \mathrm{d}z \int \mathrm{d}^2 r_\parallel \, \mathrm{e}^{i\boldsymbol{q}\,\boldsymbol{r}} \chi(\boldsymbol{r}) \tag{4.10}$$

is the Fourier transform of the perturbative potential (3.2), restricted to one layer.

To alleviate later calculations, we now number the four DWBA terms from 1 to 4, and define the corresponding wavenumbers and amplitude factors and as

$$\begin{aligned} \boldsymbol{q}^1 &\coloneqq \boldsymbol{k}_\mathrm{f}^- - \boldsymbol{k}_\mathrm{i}^-, & C^1 &\coloneqq A_\mathrm{i}^{-*} A_\mathrm{f}^-, \\ \boldsymbol{q}^2 &\coloneqq \boldsymbol{k}_\mathrm{f}^- - \boldsymbol{k}_\mathrm{i}^+, & C^2 &\coloneqq A_\mathrm{i}^{-*} A_\mathrm{f}^+, \\ \boldsymbol{q}^3 &\coloneqq \boldsymbol{k}_\mathrm{f}^+ - \boldsymbol{k}_\mathrm{i}^-, & C^3 &\coloneqq A_\mathrm{i}^{+*} A_\mathrm{f}^-, \\ \boldsymbol{q}^4 &\coloneqq \boldsymbol{k}_\mathrm{f}^+ - \boldsymbol{k}_\mathrm{i}^+, & C^4 &\coloneqq A_\mathrm{i}^{+*} A_\mathrm{f}^+. \end{aligned} \tag{4.11}$$

Accordingly, we can write (4.9) as

$$\langle \psi_\mathrm{i} | \chi | \psi_\mathrm{f} \rangle = \sum_l \sum_u C_l^u \chi_l(\boldsymbol{q}_l^u). \tag{4.12}$$

From (4.1) we see that all four wavevectors $\boldsymbol{q}^u$ have the same horizontal component,

$$\boldsymbol{q}^u = \boldsymbol{q}_\parallel + q_\perp^u \hat{\boldsymbol{z}} \tag{4.13}$$

whence the vertical components

$$\begin{aligned} q_\perp^1 &= +k_{\mathrm{f}\perp} - k_{\mathrm{i}\perp}, \\ q_\perp^2 &= +k_{\mathrm{f}\perp} + k_{\mathrm{i}\perp}, \\ q_\perp^3 &= -k_{\mathrm{f}\perp} - k_{\mathrm{i}\perp}, \\ q_\perp^4 &= -k_{\mathrm{f}\perp} + k_{\mathrm{i}\perp}. \end{aligned} \tag{4.14}$$

4.1.2 Wave propagation across layers

The plane-wave amplitudes $A_{wl}^\pm$ need to be computed recursively from layer to layer. Since these computations are identical for incident and final waves, we omit the subscript w in the remainder of this section. At layer interfaces, the optical potential changes discontinuously. From elementary quantum mechanics we know that piecewise solutions of the Schrödinger equations must be connected such that the wavefunction $\phi(\boldsymbol{r})$ and its first derivative $\boldsymbol{\nabla}\phi(\boldsymbol{r})$ evolve continuously.

To deal with the coordinate offsets introduced in (4.4), we introduce the function

$$d_l \coloneqq z_l - z_{l+1}, \tag{4.15}$$

which is the thickness of layer l, except for $l = 0$, where the special definition of z_0 (Fig. 4.1) implies $d_0 = 0$. We consider the interface between layers l and $l-1$,

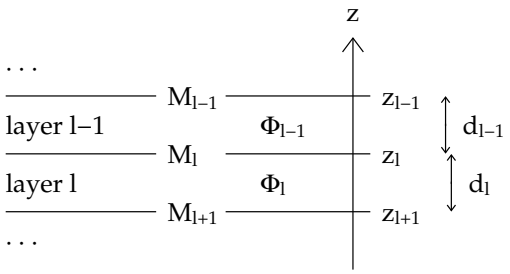

Figure 4.2: The transfer matrix M_l connects the wavefunctions Φ_l, Φ_{l-1} in adjacent layers.

with $l = 1, \ldots, N$, as shown in Fig. 4.2. This interface has the vertical coordinate $z_l = z_{l-1} - d_{l-1}$. Accordingly, the continuity conditions at the interface are

$$\begin{aligned} \phi_l(z_l) &= \phi_{l-1}(z_{l-1} - d_{l-1}), \\ \partial_z \phi_l(z_l) &= \partial_z \phi_{l-1}(z_{l-1} - d_{l-1}). \end{aligned} \tag{4.16}$$

We abbreviate

$$f_l := k_{\perp l}/K = \sqrt{n_l^2 - (k_\parallel/K)^2} \tag{4.17}$$

and

$$\delta_l := \mathrm{e}^{iKf_l d_l}. \tag{4.18}$$

For the plane waves (4.4), the continuity conditions (4.16) take the form

$$\begin{aligned} +A_l^- \quad +A_l^+ \quad &= \quad +A_{l-1}^- \delta_{l-1} \quad +A_{l-1}^+ \delta_{l-1}^*, \\ -A_l^- f_l + A_l^+ f_l \quad &= \quad -A_{l-1}^- \delta_{l-1} f_{l-1} + A_{l-1}^+ \delta_{l-1}^* f_{l-1}. \end{aligned} \tag{4.19}$$

After some lines of linear algebra, we can rewrite this equation system as

$$\begin{pmatrix} A_{l-1}^- \\ A_{l-1}^+ \end{pmatrix} = M_l \begin{pmatrix} A_l^- \\ A_l^+ \end{pmatrix} \tag{4.20}$$

with the transfer matrix

$$M_l := \begin{pmatrix} \delta_{l-1}^* & 0 \\ 0 & \delta_{l-1} \end{pmatrix} \frac{1}{2f_{l-1}} \begin{pmatrix} (f_{l-1} + f_l) & (f_{l-1} - f_l) \\ (f_{l-1} - f_l) & (f_{l-1} + f_l) \end{pmatrix}. \tag{4.21}$$

In a scattering setup, plane-wave amplitudes are subject to two boundary conditions. Let us assume that the source or the sink is located at $z > 0$. Then in the top layer, $A_0^- = 1$ is given by the incident or back-traced final plane wave. In the substrate, $A_N^+ = 0$ because there is no radiation coming from $z \to -\infty$. This leaves

us with two unkown amplitudes, the overall coefficients of transmission A_N^- and reflection A_0^+. These two unknowns are connected by a system of two linear equations,

$$\begin{pmatrix} 1 \\ A_0^+ \end{pmatrix} = M_1 \cdots M_N \begin{pmatrix} A_N^- \\ 0 \end{pmatrix}. \tag{4.22}$$

While it is possible in principle to solve this as a matrix equation, the actual implementation in `BornAgain` starts with a unit vector in the substrate, and then carries out the propagation step (4.20) interface by interface, yielding unnormalized amplitudes

$$\begin{pmatrix} \tilde{A}_l^- \\ \tilde{A}_l^+ \end{pmatrix} := M_{l+1} \cdots M_N \begin{pmatrix} 1 \\ 0 \end{pmatrix}. \tag{4.23}$$

When the top layer is reached, the obtained values are renormalized so that the boundary condition $A_0^- = 1$ be satisfied,

$$A_l^\pm = \frac{\tilde{A}_l^\pm}{\tilde{A}_0^-}. \tag{4.24}$$

For GISAS detection in transmission geometry (sink location $z < 0$) all the development following (4.21) holds with exchanged order of layers: $(0, \dots, N) \mapsto (N, \dots, 0)$.

GISAS in transmission geometry is not yet implemented in `BornAgain`, but high on our agenda.

At this point, it may be an interesting exercise to make a connection with a well known textbook result. Consider a system with a single interface between two semi-infinite media. A straightforward computation will show that the transmission and reflection probabilities determined as above agree with Fresnel's result for s-polarized light,[1]

$$|A_N^-|^2 = \left|\frac{2f_0}{f_0 + f_1}\right|^2, \quad |A_0^+|^2 = \left|\frac{f_0 - f_1}{f_0 + f_1}\right|^2. \tag{4.25}$$

The above algorithm fails if $f_l \to 0$ because M_{l+1} becomes singular. A layer with $f_l = 0$ only sustains horizontal wave propagation; radiation from below or above is totally reflected at its boundaries. In `BornAgain`, such total reflection is imposed if $|f_l|$ falls below a very small value (currently 10^{-20}). However, except for the top vacuum layer this ought to be inconsequential because the index of refraction should always have an absorptive component that prevents f_l from becoming zero.

[1] See any optics textbook, e.g. Born & Wolf [11, ch. 1.5.2] or Hecht [12, ch. 4.6.2].

4.1.3 Damped waves in absorbing media or under total reflection

In Sect. 3.2, we have chosen the horizontal wavevector $\boldsymbol{k}_\parallel$ to be always real and constant. In contrast, the vertical wavenumber $k_{\perp l}$, given by (4.2), can become imaginary or complex. If $\overline{n_l^2}$ is real and smaller than $n_0^2 \cos^2 \alpha_0$, then Snell's law of refraction (4.8) cannot be fulfilled, and the radicand in (4.2) becomes negative so that $k_{\perp l}$ becomes pure imaginary. If the layer is absorbing, described by a positive imaginary part of $\overline{n_l^2}$, then the radicand in (4.2) becomes complex, and the wavenumber $k_{\perp l}$ as well. For complex $k_{\perp l}$, the theory developed above remains applicable, except that the geometric interpretation of the wavevectors $\boldsymbol{k}_\pm$ in Eqs. (4.6–4.8) is untenable.

Writing

$$k_\perp = k'_\perp + ik''_\perp \tag{4.26}$$

for a decomposition into a real and an imaginary part, we find an exponential decay of the plane wave amplitudes

$$\left|\phi_l^\pm(z)\right| = \mathrm{e}^{\mp k''_{\perp l} z} \tag{4.27}$$

along their propagation direction $\pm z$. With an analogous decomposition of the three-dimensional wavevector (4.1), we obtain for the flux, defined as in (2.27),

$$\boldsymbol{J}_l(\boldsymbol{r}) = \boldsymbol{k}' \mathrm{e}^{-2k_{\perp l} z}. \tag{4.28}$$

In the special case of a pure imaginary $k_{\perp l}$, the flux direction is $\boldsymbol{k}' = \boldsymbol{k}_\parallel$. Then $\psi_l(\boldsymbol{r})$ is an *evanescent wave*, travelling horizontally. Since a stationary evanescent wave implies that there is no vertical energy transport, all incoming radiation undergoes *total reflection*.

In the generic case of a complex $k_{\perp l}$, the flux has a vertical component. Accordingly, the total reflection is not perfect. Some intensity is dissipated in layer l. And if layer $l < N$ is not too thick, then some radiation intensity also tunnels into the adjacent layer $l + 1$.

Chapter 5

Particle Assemblies

5.1 Embedded particles

In many important GISAS applications, fluctuations of the refractive index are due to *islands*, *inclusions* or *holes* of a mesoscopic size (nanometer to micrometer). In the following, all such inhomogeneities will be described as *particles* that are embedded in a material layer.

Documentation on inter-particle correlations is under preparation. `BornAgain` currently offers the same choice of models as `IsGISAXS`. Therefore, for the moment we refer to the `IsGISAXS` manual [7].

Implemented particle form factors are described in Appendix B.

Appendix A

Some proofs

This appendix contains proofs that were taken out of the main text in order not to disrupt the physics narration.

A.1 Source–detector reciprocity for scalar waves

We derive a source-detector reciprocity theorem for the scalar Schrödinger equation. It is needed in the derivation of the distorted-wave Born approximation (Sect. 3.1.2), where it allows us to short-cut the computation of the Green function, yielding at once the far-field at the detector position.

We start from a generic stationary Schrödinger equation with an isolated inhomogeneity,

$$\left\{\boldsymbol{\nabla}^2 + v(\boldsymbol{r})\right\} G(\boldsymbol{r}, \boldsymbol{r}_\mathrm{S}) = \delta(\boldsymbol{r} - \boldsymbol{r}_\mathrm{S}). \tag{A.1}$$

We assume that the source location $\boldsymbol{r}_\mathrm{S}$ (which in our application is a scattering center) lies within a finite sample volume. Outside the sample, the potential $v(\boldsymbol{r})$ has the constant value K^2 so that (A.1) reduces to the Helmholtz equation

$$\left\{\boldsymbol{\nabla}^2 + K^2\right\} G(\boldsymbol{r}, \boldsymbol{r}_\mathrm{S}) = 0. \tag{A.2}$$

We introduce the adjoint Green function B that originates from a source term at the detector location and obeys

$$\left\{\boldsymbol{\nabla}^2 + v(\boldsymbol{r})\right\} B(\boldsymbol{r}, \boldsymbol{r}_\mathrm{D}) = \delta(\boldsymbol{r} - \boldsymbol{r}_\mathrm{D}). \tag{A.3}$$

We also introduce the auxiliary vector field

$$\boldsymbol{X}(\boldsymbol{r}, \boldsymbol{r}_\mathrm{S}, \boldsymbol{r}_\mathrm{D}) := B(\boldsymbol{r}, \boldsymbol{r}_\mathrm{D})\boldsymbol{\nabla} G(\boldsymbol{r}, \boldsymbol{r}_\mathrm{S}) - G(\boldsymbol{r}, \boldsymbol{r}_\mathrm{S})\boldsymbol{\nabla} B(\boldsymbol{r}, \boldsymbol{r}_\mathrm{D}). \tag{A.4}$$

We inscribe the sample, the detector, and the origin of the coordinate system into a sphere $\mathcal{S}$ with radius R, and compute the volume integral

$$\begin{aligned} I(\boldsymbol{r}_\mathrm{S}, \boldsymbol{r}_\mathrm{D}) &= \int_{\mathcal{S}} \mathrm{d}^3 r\, \boldsymbol{\nabla} \boldsymbol{X}(\boldsymbol{r}, \boldsymbol{r}_\mathrm{S}, \boldsymbol{r}_\mathrm{D}) \\ &= \int_{\mathcal{S}} \mathrm{d}^3 r\, \left(B\boldsymbol{\nabla}^2 G - G\boldsymbol{\nabla}^2 B\right) \\ &= B(\boldsymbol{r}_\mathrm{S}, \boldsymbol{r}_\mathrm{D}) - G(\boldsymbol{r}_\mathrm{D}, \boldsymbol{r}_\mathrm{S}). \end{aligned} \tag{A.5}$$

Alternatively, we can compute I as a surface integral

$$I(\boldsymbol{r}_\mathrm{S}, \boldsymbol{r}_\mathrm{D}) = \int_{\partial\mathcal{S}} \mathrm{d}\boldsymbol{\sigma}\, \boldsymbol{X}(\boldsymbol{r}, \boldsymbol{r}_\mathrm{S}, \boldsymbol{r}_\mathrm{D}) = \int_{\partial\mathcal{S}} \mathrm{d}\sigma\, \left(B\partial_R G - G\partial_R B\right). \tag{A.6}$$

On the surface $\partial\mathcal{S}$, B and G are outgoing wave fields that obey the Helmholtz equation. Solutions of this equation in spherical coordinates have a well-known series expansion. We send $R \to \infty$ so that we need only to retain the lowest order, the form of which has been anticipated in the boundary condition (2.9),

$$G(\boldsymbol{r}(R, \vartheta, \varphi), \boldsymbol{r}_\mathrm{S}) \doteq \frac{\mathrm{e}^{iKR}}{4\pi R} g(\vartheta, \varphi), \tag{A.7}$$

and similarly

$$B(\boldsymbol{r}(R, \vartheta, \varphi), \boldsymbol{r}_\mathrm{D}) \doteq \frac{\mathrm{e}^{iKR}}{4\pi R} b(\vartheta, \varphi). \tag{A.8}$$

The functions g and b can be further expanded into spherical harmonics, but this is of no interest here. The decisive point is the factorization of G and B and their common R dependence. It follows at once that

$$I(\boldsymbol{r}_\mathrm{S}, \boldsymbol{r}_\mathrm{D}) = \int_{\partial\mathcal{S}} \mathrm{d}\sigma\, (R\text{-dependent})(bg - gb) = 0. \tag{A.9}$$

From (A.5) we obtain the *reciprocity theorem*

$$G(\boldsymbol{r}_\mathrm{D}, \boldsymbol{r}_\mathrm{S}) = B(\boldsymbol{r}_\mathrm{S}, \boldsymbol{r}_\mathrm{D}). \tag{A.10}$$

It allows us to obtain the far-field value of the forward-propagating Green function G at the detector position $\boldsymbol{r}_\mathrm{D}$ from the adjoint Green function B that traces the radiation back from $\boldsymbol{r}_\mathrm{D}$ to the source location $\boldsymbol{r}_\mathrm{S}$. The theorem is practically important because B is much easier to compute than the unexpanded G.

Appendix B

Form factor library

`BornAgain` comes with a comprehensive collection of hard-coded shape transforms for standard particle geometries like spheres, cylinders, prisms, pyramids or ripples. This collection is documented in the following. For each shape, the real-space geometry is shown in orthogonal projections, the parameters of the `BornAgain` method are defined, an analytical expression for the form factor is given, and exemplary results for $|F(\boldsymbol{q})|^2$ versus $\alpha_\mathrm{f}, \phi_\mathrm{f}$ are shown for small-angle scattering conditions ($\alpha_\mathrm{i} = \phi_\mathrm{i} = 0$).

The computation of $F(\boldsymbol{q})$ is based on shapes $S(\boldsymbol{r})$ given in Cartesian coordinates, as defined in the orthogonal projections. Typically, the vertical (z) direction is chosen along a symmetry axis of the particle. The origin is always at the center of the bottom side of the particle. Different parametrization or a different choice of the origin cause our analytic form factors to trivially deviate from expressions given in the `IsGISAXS` manual [7, Sect. 2.3] or in the literature [8, Appendix].

We recomputed all expressions to make sure that they also hold for complex scattering vectors, used to describe in order to take any material absorption into account. The implementation in `BornAgain` allows all three components of $\boldsymbol{q}$ to be complex. According to Sect. 4.1.3, only the vertical components of $\boldsymbol{k}_\mathrm{i}$ and $\boldsymbol{k}_\mathrm{f}$ can have imaginary parts. However, to account for a tilt of the particle, it may be necessary to evaluate $F(\tilde{\boldsymbol{q}})$ with a rotated scattering vector $\tilde{\boldsymbol{q}}$ that has complex $\tilde{q}_x$ or $\tilde{q}_y$.

The following tables summarize the implemented particle geometries, roughly ordered by decreasing symmetry. Afterwards, the detailed documentation is in alphabetical order.

Shape	Name	Symmetry	Parameters	Reference
	`FullSphere`	R_3	R	Page 48
	`FullSpheroid`	$\mathrm{D}_{\infty\mathrm{h}}$	R, H	Page 52
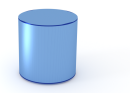	`Cylinder`	$\mathrm{D}_{\infty\mathrm{h}}$	R, H	Page 44

	`TruncatedSphere`	$C_{\infty v}$	R, H	Page 70
	`TruncatedSpheroid`	$C_{\infty v}$	R, H, f_p	Page 72
	`Cone`	$C_{\infty v}$	R, H, α	Page 38
	`TruncatedCube`	O_h	L, t	Page 66
	`Prism6`	D_{6h}	R, H	Page 56
	`Cone6`	C_{6v}	R, H, α	Page 40
	`Pyramid`	C_{4v}	L, H, α	Page 58
	`Cuboctahedron`	C_{4v}	L, H, r_H, α	Page 42
	`Prism3`	D_{3h}	L, H	Page 54
	`Tetrahedron`	C_{3v}	L, H, α	Page 64
	`EllipsoidalCylinder`	D_{2h}	R_a, R_b, H	Page 46
	`Box`	D_{2h}	L, W, H	Page 36
	`HemiEllipsoid`	C_{2v}	R_a, R_b, H	Page 50
	`AnisoPyramid`	C_{2v}	L, W, H, α	Page 34
	`Ripple1`	C_{2v}	L, W, H	Page 60
	`Ripple2`	C_s	L, W, H, d	Page 62

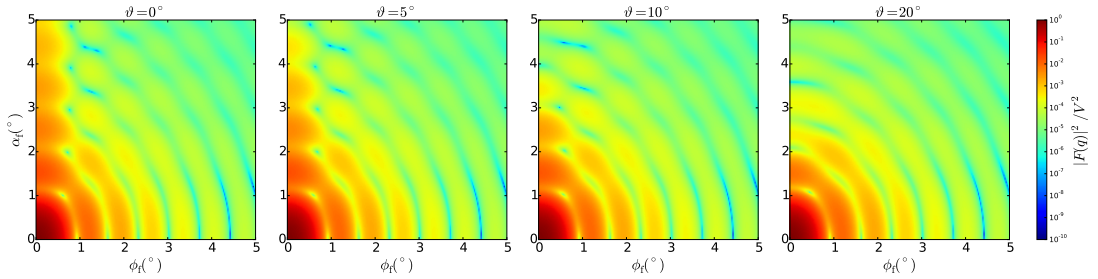

Figure B.1: Normalized intensity $I(\alpha_\mathrm{f}, \phi_\mathrm{f})$ for small-angle scattering by a truncated sphere with $R = 4.2$ nm and $H = 6.1$ nm, for four different tilt angles ϑ (rotation around the y axis). Since I possess the standard symmetry (B.2), data are only shown for first quadrant $0^\circ \leq \phi_\mathrm{f}, \alpha_\mathrm{f} \leq 5^\circ$.

In the following subsections, information about the implemented geometries is given in standardized form. Analytical expressions are given for the form factor $F(\boldsymbol{q})$, for the volume $V = F(0)$, and for the maximum horizontal section S (the area of the particle as seen from above). Mathematical notation in the form factor expressions includes the cardinal sine functions $\mathrm{sinc}(z) := \sin(z)/z$ and the Bessel function of first kind and first order $J_1(z)$ [13, Ch. 9]. If results contain an integral, then no analytical form was found, and the integral is evaluated by numeric quadrature. The analytical expressions for $F(\boldsymbol{q})$ contain singularities for certain values of $\boldsymbol{q}$. All these singularities are removable. Our implementation comprises appropriate case distinctions.

Geometrical objects can be parametrized in different ways. Concerns about user experience and about code readability sometimes lead to different choices. For the `Born Again` user interfaces (GUI and API) we have chosen the most standard parameters, as used in elementary geometry, like length, height, radius, even if this is at variance from the `IsGISAXS` precedent. Where our parametrization made analytic expressions too tedious, we use alternate internal parameters to alleviate the formulæ.

Examplary form factors are numerically computed in Born approximation. The particles are assigned a refractive index of $n = 10^{-5}$. Parameters are chosen such that the particle volume V is about 250 nm^3 (within ± 5 %); except ripples, which are chosen with a vertical section V/L of 40 nm^2 and a length of 25 nm. The incident wavelength is 1 Å. The incident beam is always in x direction, hence $\alpha_\mathrm{i} = \phi_\mathrm{i} = 0$. Simulated detector images are normalized to the maximum scattering intensity at $F(0) = V$,

$$I(\alpha_\mathrm{f}, \phi_\mathrm{f}) := |F(q(\alpha_\mathrm{f}, \phi_\mathrm{f}))|^2 / V^2. \tag{B.1}$$

All plots have the same logarithmic color scale, extending over ten decades from $10^{-1)}$ to 1. Plot ranges in α_f and ϕ_f are also standardized as far as reasonably possible. For most particle geometries, I has horizontal and vertical mirror planes:

$$I(\alpha_\mathrm{f}, \phi_\mathrm{f}) = I(\alpha_\mathrm{f}, -\phi_\mathrm{f}) = I(-\alpha_\mathrm{f}, -\phi_\mathrm{f}) = I(\alpha_\mathrm{f}, -\phi_\mathrm{f}). \tag{B.2}$$

For these particles, plots of I are restricted to the quadrant $\alpha_\mathrm{f} \geq 0$, $\phi_\mathrm{f} \geq 0$. However, it requires some experience to fully appreciate the information content of these plots. For

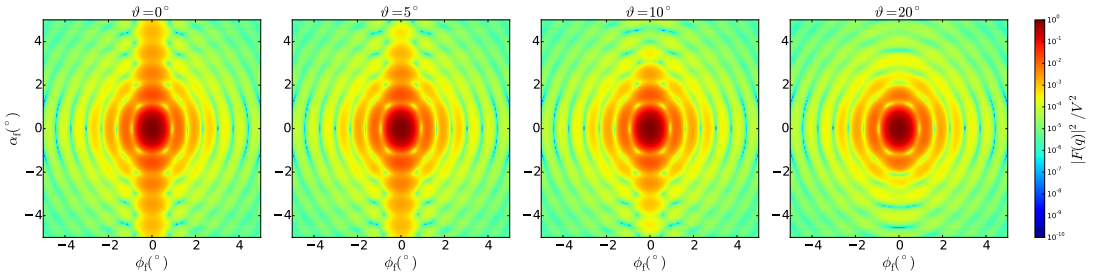

Figure B.2: Same data as in Fig. B.1, but now shown for all four quadrants ($-5^\circ \leq \phi_\mathrm{f}, \alpha_\mathrm{f} \leq 5^\circ$). The vertical interference pattern, which gradually disappears with increasing tilt angle, is much more salient in this plot than in the preceding one-quadrant representation.

a demonstration of this, try to capture the main features of Fig. B.1. Then compare with Fig. B.2.

B.1 AnisoPyramid (rectangle-based)

Real-space geometry

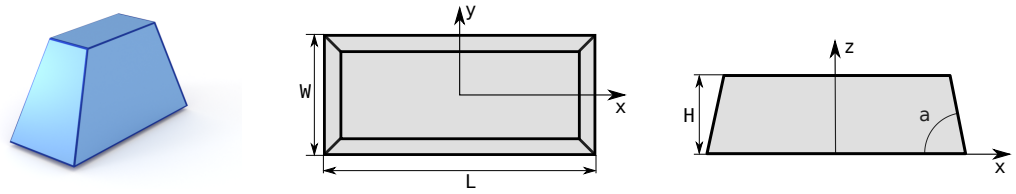

Perspective Top view Side view

Figure B.3: A truncated pyramid with a rectangular base.

Syntax and parameters

```
FormFactorAnisoPyramid(length, width, height, alpha)
```

with the parameters

- `length` of the base, L,
- `width` of the base, W,
- `height`, H
- `alpha`, angle between the base and a side face, α.

They must fulfill

$$H \leq \frac{\tan\alpha}{2} L \quad \text{and} \quad H \leq \frac{\tan\alpha}{2} W$$

Form factor etc

Notation:

$$\ell := L/2, \quad w := W/2, \quad h := H/2, \quad f_{\pm}(z) := \exp(\pm iz)\,\mathrm{sinc}(z).$$

Results:

$$\begin{aligned} F = \frac{H}{q_x q_y}\Big\{ & +f_+\left(\left(\frac{q_x - q_y}{\tan\alpha} + q_z\right)h\right)\exp(-i(q_x\ell - q_y w)) \\ & +f_-\left(\left(\frac{q_x - q_y}{\tan\alpha} - q_z\right)h\right)\exp(+i(q_x\ell - q_y w)) \\ & -f_+\left(\left(\frac{q_x + q_y}{\tan\alpha} + q_z\right)h\right)\exp(-i(q_x\ell + q_y w)) \\ & -f_-\left(\left(\frac{q_x + q_y}{\tan\alpha} - q_z\right)h\right)\exp(+i(q_x\ell + q_y w))\Big\}, \end{aligned}$$

$$V = H\Big[LW - \frac{(L+W)H}{\tan\alpha} + \frac{4}{3}\frac{H^2}{\tan^2\alpha}\Big].$$
$$S = LW.$$

Examples

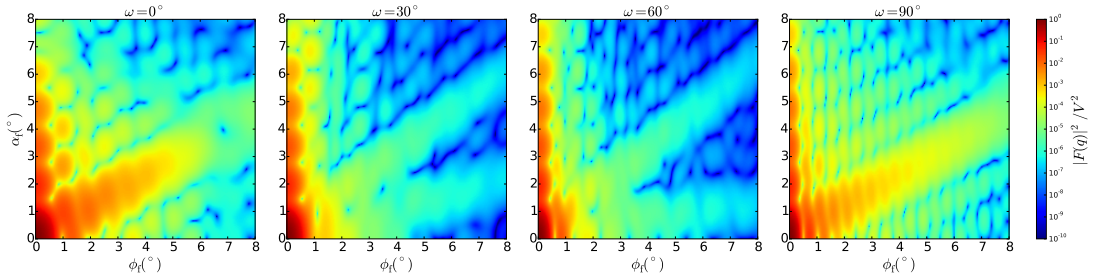

Figure B.4: Normalized intensity $|F|^2/V^2$, computed with $L = 13$ nm, $W = 8$ nm, $H = 4.2$ nm, and $\alpha = 60°$, for four different angles ω of rotation around the z axis.

References

Agrees with the *In-plane anisotropic pyramid* form factor of `IsGISAXS` [7, Eq. 2.40] [8, Eq. 217], except for different parametrization and for a refactoring of the analytical expression for $F(\boldsymbol{q})$. This is *not* the *anisotropic pyramid* of `FitGISAXS`, which is a true pyramid with an off-center apex [14].

B.2 Box (cuboid)

Real-space geometry

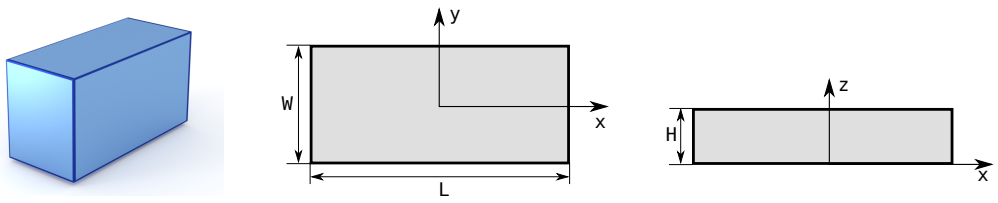

Perspective Top view Side view

Figure B.5: A rectangular cuboid.

Syntax and parameters

```
FormFactorBox(length, width, height)
```

with the parameters

- `length` of the base, L,
- `width` of the base, W,
- `height`, H.

Form factor etc

$$F = LWH \exp\left(iq_z \frac{H}{2}\right) \operatorname{sinc}\left(q_x \frac{L}{2}\right) \operatorname{sinc}\left(q_y \frac{W}{2}\right) \operatorname{sinc}\left(q_z \frac{H}{2}\right),$$

$$V = LWH,$$

$$S = LW.$$

Examples

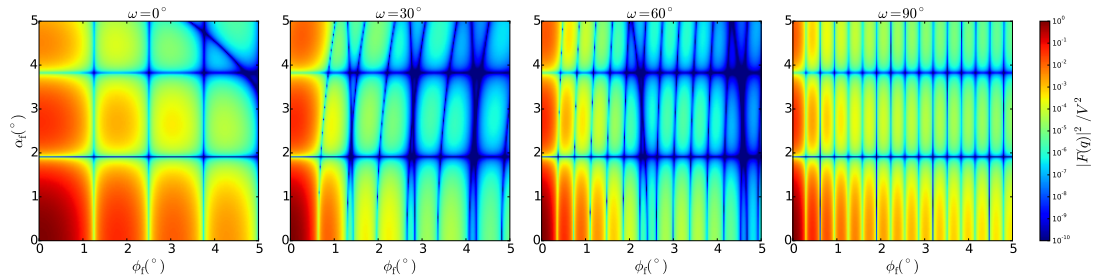

Figure B.6: Normalized intensity $|F|^2/V^2$, computed with $L = 18$ nm, $W = 4.6$ nm, and $H = 3$ nm, for four different angles ω of rotation around the z axis.

References

Agrees with *Box* form factor of `IsGISAXS` [7, Eq. 2.38] [8, Eq. 214], except for factors 1/2 in the definitions of parameters L, W, H.

B.3 Cone (circular)

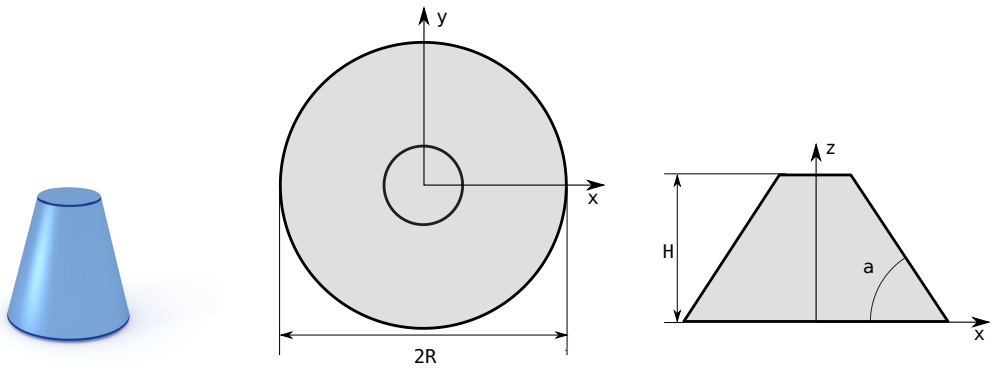

Perspective Top view Side view

Figure B.7: A truncated cone with circular base.

Real-space geometry

Syntax and parameters

```
FormFactorCone(radius, height, alpha)
```

with the parameters

- `radius`, R,
- `height`, H,
- `alpha`, angle between the side and the base, α.

They must fulfill

$$H \leq R \tan \alpha.$$

Form factor etc

Notation:

$$R_H := R - \frac{H}{\tan \alpha}, \quad q_\parallel := \sqrt{q_x^2 + q_y^2}, \quad \tilde{q}_z := q_z \tan \alpha.$$

Results:

$$F = 2\pi \tan \alpha \, \mathrm{e}^{i \tilde{q}_z R} \int_{R_H}^{R} \mathrm{d}\rho \, \rho^2 \frac{J_1(q_\parallel \rho)}{q_\parallel \rho} \mathrm{e}^{-i \tilde{q}_z \rho},$$

$$V = \frac{\pi}{3} \tan \alpha \left(R^3 - R_H^3\right),$$

$$S = \pi R^2.$$

Examples

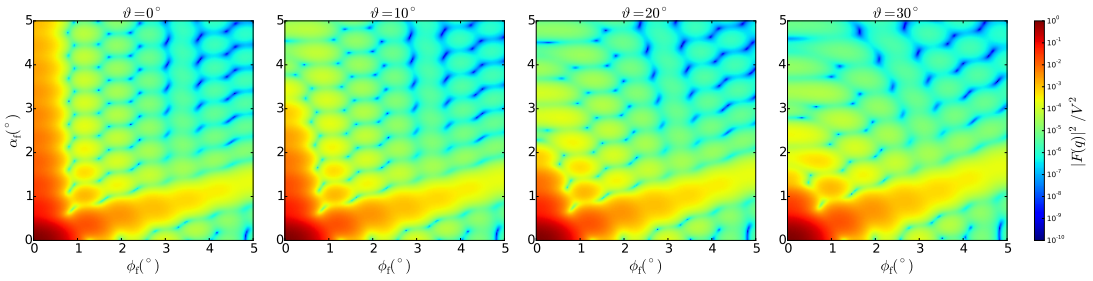

Figure B.8: Normalized intensity $|F|^2/V^2$, computed with $R = 4$ nm, $H = 11$ nm, and $\alpha = 75^\circ$, for four different tilt angles ϑ (rotation around the y axis).

References

Agrees with *Cone* form factor of `IsGISAXS` [7, Eq. 2.28] [8, Eq. 225], except for a substitution $z \to \rho$ in our expression for F.

B.4 Cone6 (hexagonal)

Real-space geometry

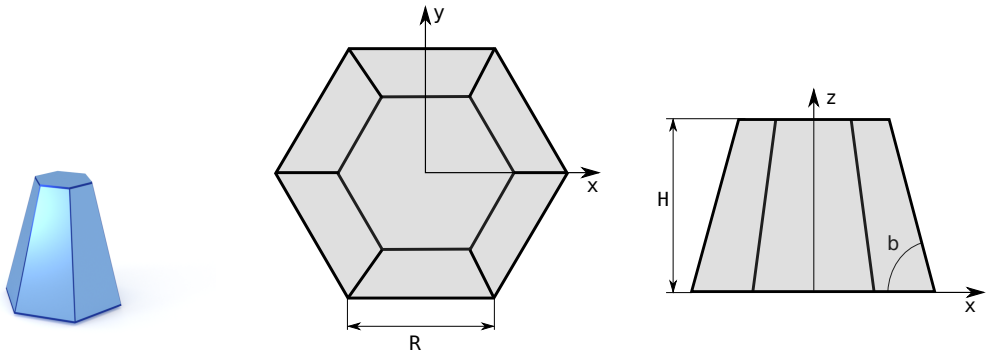

Figure B.9: A truncated hexagonal pyramid.

Syntax and parameters

```
FormFactorCone6(radius,height, alpha)
```

with the parameters

- `radius` of the regular hexagonal base, R,
- `height`, H,
- `alpha`, between the base and a side face, α.

Note that the orthographic projection does not show α, but the angle β between the base and a side edge. They are related through $\sqrt{3}\tan\alpha = 2\tan\beta$. The following is written more conveniently in terms of β. The parameters must fulfill

$$H \leq (\tan\beta)R.$$

Form factor etc

Notation:

$$R_H := R - \frac{H}{\tan\beta}, \quad \tilde{q}_x := \frac{1}{2}q_y, \quad \tilde{q}_y := \frac{\sqrt{3}}{2}q_y, \quad \tilde{q}_z := (\tan\beta)q_z.$$

Results:

The integral in F could be worked out algebraically.

$$F = \frac{\sqrt{3}\,\mathrm{e}^{i\tilde{q}_z R}}{\tilde{q}_y^2 - \tilde{q}_x^2} \int_{R_H}^{R} \mathrm{d}\rho\, \mathrm{e}^{-i\tilde{q}_z\rho} \Big[\rho\tilde{q}_y \,\mathrm{sinc}(\tilde{q}_x\rho)\sin(\tilde{q}_y\rho) + \cos(2\tilde{q}_x\rho) - \cos(\tilde{q}_y\rho)\cos(\tilde{q}_x\rho)\Big],$$

$$V = \tan\beta\,(R^3 - R_H^3)\,,$$

$$S = \frac{3\sqrt{3}R^2}{2}.$$

Examples

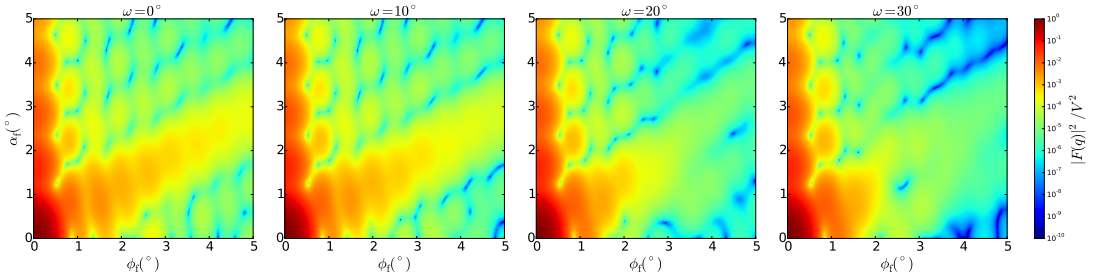

Figure B.10: Normalized intensity $|F|^2/V^2$, computed with $R = 6$ nm, $H = 5$ nm, and $\alpha = 60°$, for four different angles ω of rotation around the z axis.

References

Hopefully agrees with *Cone6* form factor of `IsGISAXS` [7, Eq. 2.32] [8, Eq. 222], except for different parametrization.

B.5 Cuboctahedron

Real-space geometry

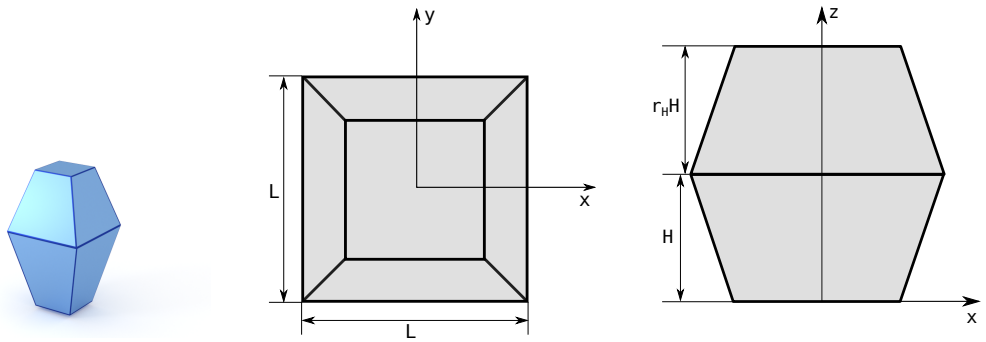

Perspective Top view Side view

Figure B.11: A compound of two truncated pyramids with a common square base and opposite orientations.

Syntax and parameters

```
FormFactorCuboctahedron(length, height, height_ratio, alpha)
```

with the parameters

- `length` of the shared square base, L,
- `height` of the bottom pyramid, H,
- `height_ratio` between the top and the bottom pyramid, r_H,
- `alpha`, angle between the base and a side face, α.

They must fulfill

$$H \leq \frac{\tan\alpha}{2} L \quad \text{and} \quad r_h H \leq \frac{\tan\alpha}{2} L.$$

Form factor etc

Using the form factor of a square pyramid F_{Py} (Sect. B.13):

$$F = \exp(iq_z H)\Big[F_{\mathrm{Py}}(q_x, q_y, q_z, L, r_H H, \alpha) + F_{\mathrm{Py}}(q_x, q_y, -q_z, L, H, \alpha))\Big],$$

$$V = \frac{1}{6}\tan(\alpha) L^3 \left[2 - \left(1 - \frac{2H}{L\tan(\alpha)}\right)^3 - \left(1 - \frac{2r_H H}{L\tan(\alpha)}\right)^3\right],$$

$$S = L^2.$$

Examples

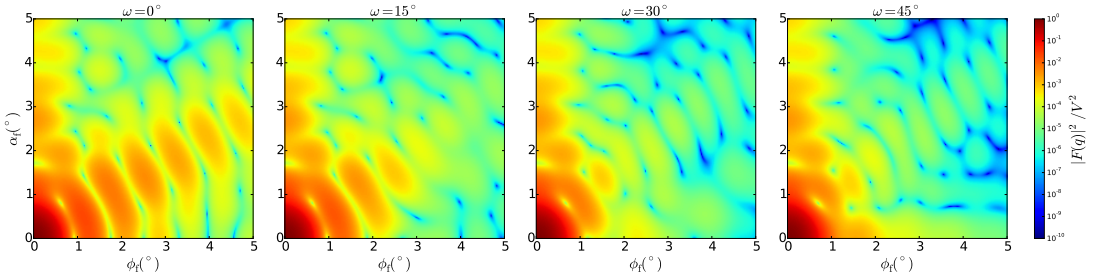

Figure B.12: Normalized intensity $|F|^2/V^2$, computed with $L = 8$ nm, $H = 5$ nm, $r_H = 0.5$, and $\alpha = 60°$, for four different angles ω of rotation around the z axis.

References

Agrees with *Cuboctahedron* form factor of `IsGISAXS` [7, Eq. 2.34] [8, Eq. 218], except for different parametrization $L = 2R_{\texttt{IsGISAXS}}$.

B.6 Cylinder

Real-space geometry

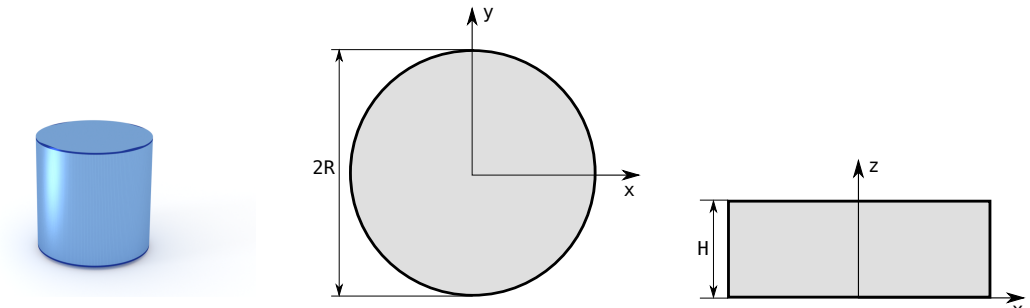

Perspective Top view Side view

Figure B.13: An upright circular cylinder.

Syntax and parameters

```
FormFactorCylinder(radius, height)
```

with the parameters

- `radius` of the circular base, R,
- `height`, H.

Form factor etc

Notation:

$$q_{\parallel} := \sqrt{q_x^2 + q_y^2}.$$

Results:

$$F = 2\pi R^2 H \,\mathrm{sinc}\left(q_z \frac{H}{2}\right) \exp\left(i q_z \frac{H}{2}\right) \frac{J_1(q_{\parallel} R)}{q_{\parallel} R},$$

$$V = \pi R^2 H,$$

$$S = \pi R^2.$$

Examples

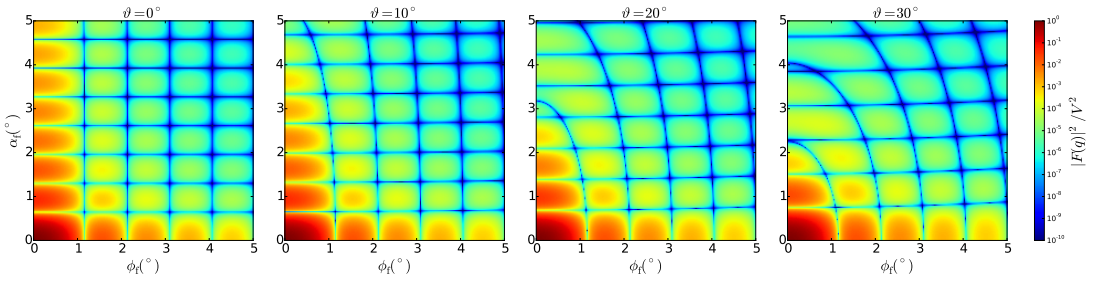

Figure B.14: Normalized intensity $|F|^2/V^2$, computed with $R = 3$ nm and $H = 8.8$ nm, for four different tilt angles ϑ (rotation around the y axis).

References

Agrees with *Cylinder* form factor of `IsGISAXS` [7, Eq. 2.27] [8, Eq. 223].

B.7 EllipsoidalCylinder

Real-space geometry

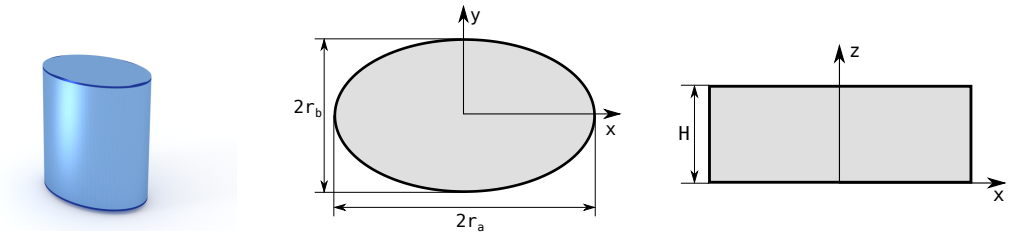

Perspective Top view Side view

Figure B.15: A upright cylinder whose cross section is an ellipse.

Syntax and parameters

```
FormFactorEllipsoidalCylinder(radius_a, radius_b, height)
```

with the parameters

- `radius_a`, in x direction, R_a,
- `radius_b`, in y direction, R_b,
- `height`, H.

Form factor etc

Notation:

$$\gamma := \sqrt{(q_x R_a)^2 + (q_y R_b)^2}$$

Results:

$$F = 2\pi R_a R_b H \exp\left(i\frac{q_z H}{2}\right) \operatorname{sinc}\left(\frac{q_z H}{2}\right) \frac{J_1(\gamma)}{\gamma},$$

$$V = \pi R_a R_b H,$$

$$S = R_a R_b.$$

Examples

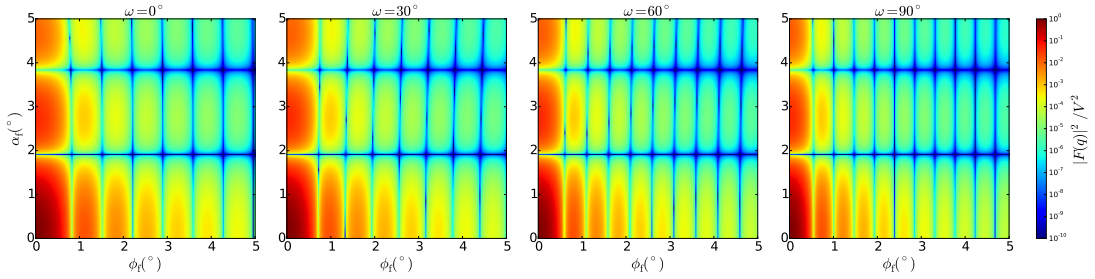

Figure B.16: Normalized intensity $|F|^2/V^2$, computed with $R_a = 6.3$ nm, $R_b = 4.2$ nm and $H = 3$ nm, for four different angles ω of rotation around the z axis.

References

Agrees with the `IsGISAXS` form factor *Ellipsoid* [7, Eq. 2.41, wrongly labeled in Fig. 2.4] or *Ellipsoidal Cylinder* [8, Eq. 224].

B.8 FullSphere

Real-space geometry

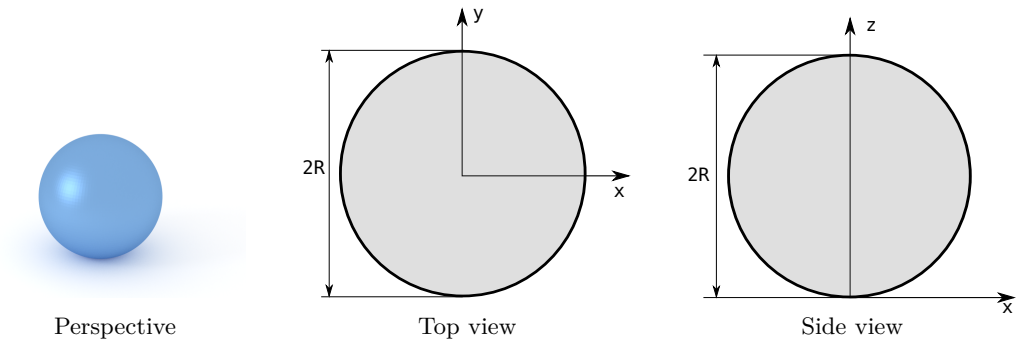

Perspective Top view Side view

Figure B.17: A full sphere.

Syntax and parameters

```
FormFactorFullSphere(radius)
```

with the parameter

- `radius`, R.

Form factor etc

$$F = 4\pi R^3 \exp(iq_z R)\frac{\sin(qR) - qR\cos(qR)}{(qR)^3},$$

$$V = \frac{4\pi}{3}R^3,$$

$$S = \pi R^2.$$

Example

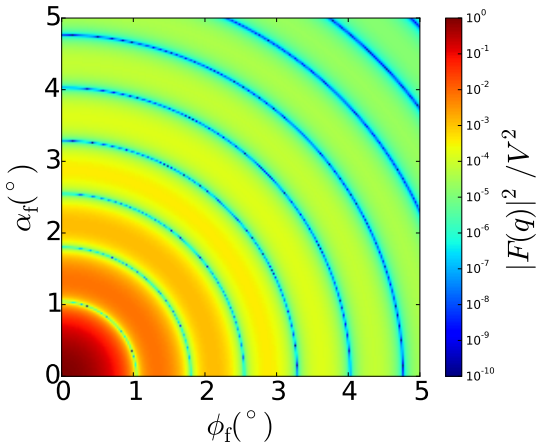

Figure B.18: Normalized intensity $|F|^2/V^2$, computed with $R = 3.9$ nm.

References

This form factor, which certainly goes back at least to Lord Rayleigh, agrees with the *Full sphere* of `IsGISAXS`[7, Eq. 2.36] [8, Eq. 226].

B.9 HemiEllipsoid

Real-space geometry

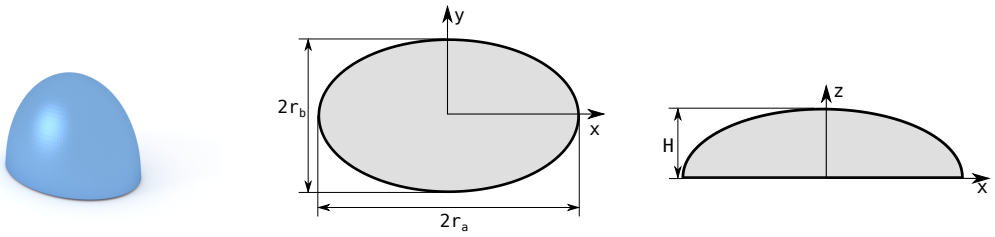

Perspective Top view Side view

Figure B.19: An horizontally oriented ellipsoid, truncated at the central plane.

Syntax and parameters

```
FormFactorHemiEllipsoid(radius_a, radius_b, height)
```

with the parameters

- `radius_a`, in x direction, R_a,
- `radius_b`, in y direction, R_b,
- `height`, equal to radius in z direction, H

Form factor etc

Notation:

$$r_{a,z} := R_a\sqrt{1-\left(\frac{z}{H}\right)^2}, \quad r_{b,z} := R_b\sqrt{1-\left(\frac{z}{H}\right)^2}, \quad \gamma_z = \sqrt{(q_x r_{a,z})^2 + (q_y r_{b,z})^2}.$$

Results:

$$F = 2\pi \int_0^H \mathrm{d}z\, r_{a,z} r_{b,z} \frac{J_1(\gamma_z)}{\gamma_z} \exp(iq_z z),$$

$$V = \frac{2}{3}\pi R_a R_b H,$$

$$S = \pi R_a R_b.$$

Examples

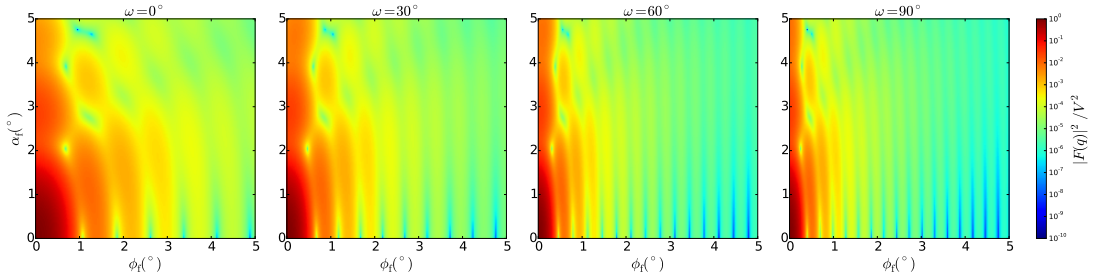

Figure B.20: Normalized intensity $|F|^2/V^2$, computed with $R_a = 10$ nm, $R_b = 3.8$ nm and $H = 3.2$ nm, for four different angles ω of rotation around the z axis.

References

Agrees with the `IsGISAXS` form factor *Anisotropic hemi-ellipsoid* [7, Eq. 2.42, with wrong sign in the z-dependent phase factor] or *Hemi-spheroid* [8, Eq. 229].

B.10 FullSpheroid

Real-space geometry

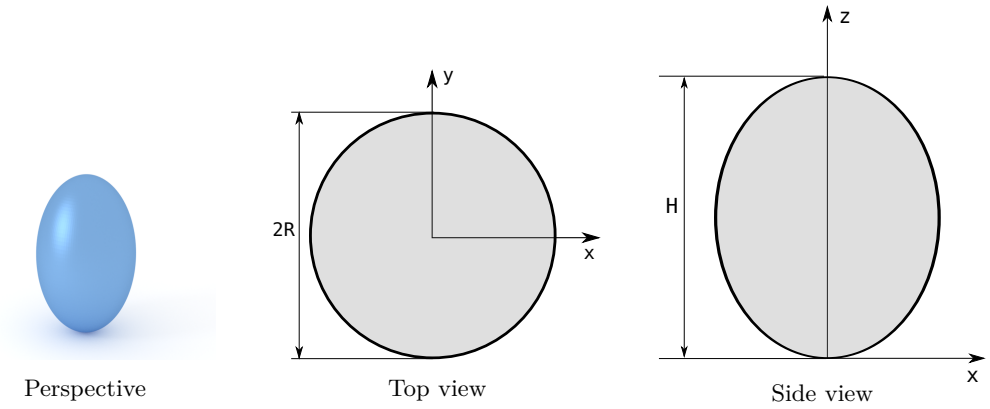

Figure B.21: A full spheroid, generated by rotating an ellipse around the vertical axis.

Syntax and parameters

```
FormFactorFullSpheroid(radius,height)
```

with the parameters

- `radius`, R,
- `height`, H.

Form factor etc

Notation:

$$R_z := R\sqrt{1-\frac{4z^2}{H^2}}, \quad q_\parallel := \sqrt{q_x^2+q_y^2}.$$

Results:

$$F = 4\pi \exp(iq_z H/2) \int_0^{H/2} \mathrm{d}z\, R_z^2 \frac{J_1(q_\parallel R_z)}{q_\parallel R_z} \cos(q_z z),$$

$$V = \frac{2}{3}R^2 H,$$

$$S = \pi R^2.$$

Example

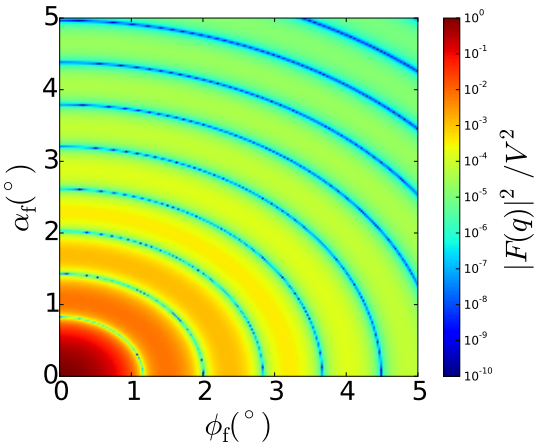

Figure B.22: Normalized intensity $|F|^2/V^2$, computed with $R = 3.5$ nm and $H = 9.8$ nm.

References

Agrees with the *Full spheroid* form factor of `IsGISAXS` [7, Eq. 2.37] [8, Eq. 227], with corrected volume formula. We also discovered a wrong factor of 2 in the `IsGISAXS` code.

B.11 Prism3 (triangular)

Real-space geometry

probably the xy view needs to be rotated by 30°

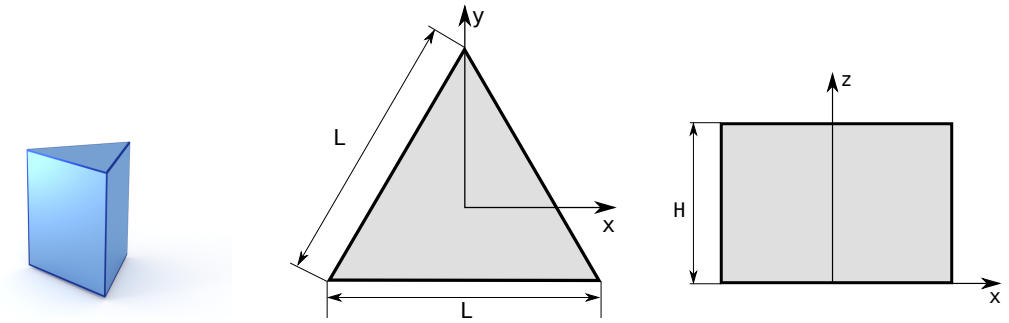

Perspective Top view Side view

Figure B.23: A prism based on an equilateral triangle.

Syntax and parameters

```
FormFactorPrism3(length, height)
```

with the parameters

- `length` of one base edge, L,
- `height`, H.

Form factor etc

$$F = \frac{2\sqrt{3}}{q_x^2 - 3q_y^2} \exp\left(-iq_y \frac{L}{2\sqrt{3}}\right) \left[\exp\left(i\sqrt{3}q_y \frac{L}{2}\right) - \cos\left(q_x \frac{L}{2}\right) - i\sqrt{3}q_y \frac{L}{2} \operatorname{sinc}\left(q_x \frac{L}{2}\right)\right] \times H \operatorname{sinc}\left(q_z \frac{H}{2}\right) \exp\left(iq_z \frac{H}{2}\right),$$

$$V = \frac{\sqrt{3}}{4} H L^2,$$

$$S = \frac{\sqrt{3}}{4} L^2.$$

Examples

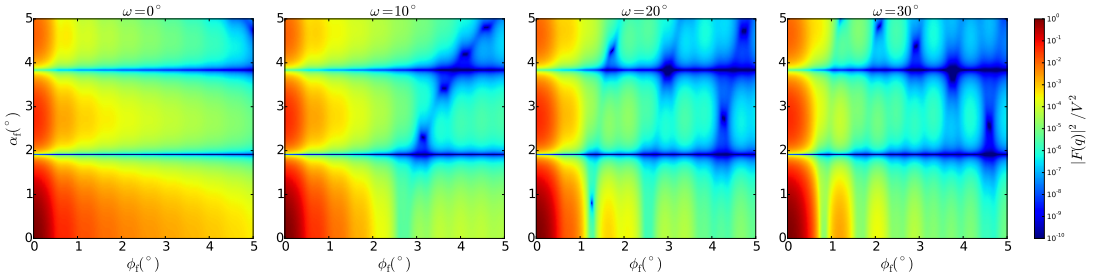

Figure B.24: Normalized intensity $|F|^2/V^2$, computed with $R = 13.8$ nm and $H = 3$ nm, for four different angles ω of rotation around the z axis.

References

Agrees with *Prism3* form factor of `IsGISAXS` [7, Eq. 2.29] [8, Eq. 219], except for the definition of parameter $L = 2R_{\texttt{IsGISAXS}}$. In `FitGISAXS` just called *Prism* [14].

B.12 Prism6 (hexagonal)

Real-space geometry

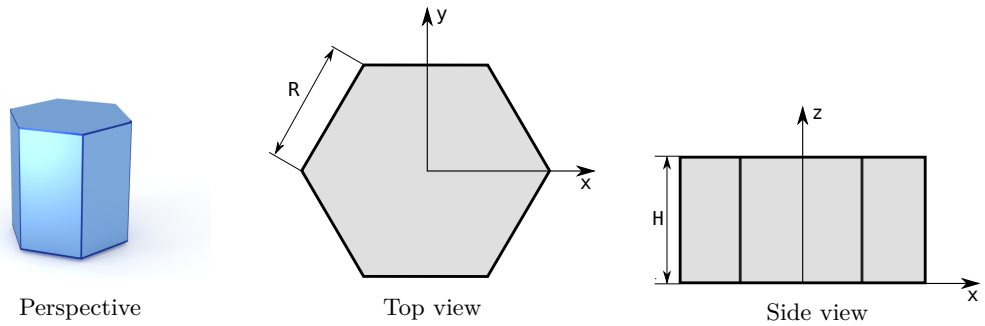

Figure B.25: A prism based on a regular hexagon.

Syntax and parameters

```
FormFactorPrism6(radius, height)
```

with the parameters

- `radius` of the hexagonal base, R,
- `height`, H.

Form factor etc

$$F = \frac{4H\sqrt{3}}{3q_y^2 - q_x^2} \operatorname{sinc}\left(q_z \frac{H}{2}\right) \exp\left(-iq_z \frac{H}{2}\right) \times \left\{ \frac{3q_y^2 R^2}{4} \operatorname{sinc}\left(\frac{q_x R}{2}\right) \operatorname{sinc}\left(\frac{\sqrt{3}q_y R}{2}\right) + \cos(q_x R) - \cos\left(q_y \frac{\sqrt{3}R}{2}\right) \cos\left(\frac{q_x R}{2}\right) \right\},$$

$$V = \frac{3\sqrt{3}}{2} H R^2,$$

$$S = \frac{3\sqrt{3}R^2}{2}.$$

Examples

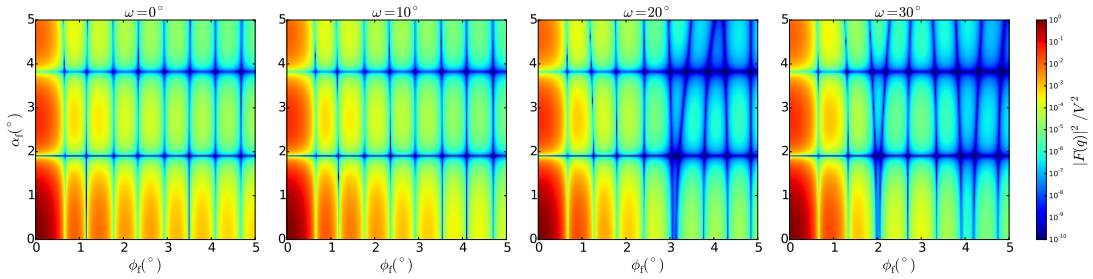

Figure B.26: Normalized intensity $|F|^2/V^2$, computed with $R = 5.7$ nm and $H = 3$ nm, for four different angles ω of rotation around the z axis.

References

Corresponds to *Prism6* form factor of `IsGISAXS` [7, Eq. 2.31] [8, Eq. 221], which has different parametrization and lacks a factor H in $F(\boldsymbol{q})$.

B.13 Pyramid (square-based)

Real-space geometry

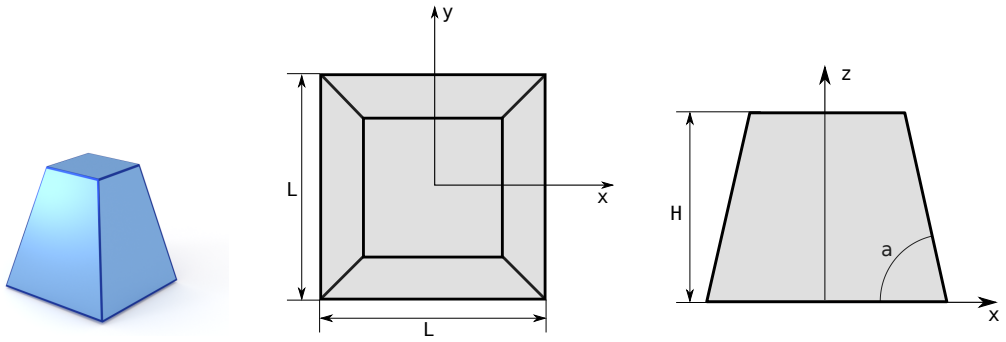

Figure B.27: A truncated pyramid with a square base.

Syntax and parameters

```
FormFactorPyramid(length, height, alpha)
```

with the parameters

- `length` of one edge of the square base, L,
- `height`, H,
- `alpha`, angle between the base and a side face, α,

They must fulfill

$$H \leq \frac{\tan\alpha}{2} L.$$

Form factor etc

Notation:

$$\ell := L/2, \quad h := H/2, \quad f_{\pm}(z) := \exp(\pm iz)\,\mathrm{sinc}(z).$$

Results:

$$\begin{aligned} F = \frac{H}{q_x q_y}\Big\{ &+f_+\left(\left(\frac{q_x - q_y}{\tan\alpha} + q_z\right)h\right)\exp(-i(q_x - q_y)\ell) \\ &+f_-\left(\left(\frac{q_x - q_y}{\tan\alpha} - q_z\right)h\right)\exp(+i(q_x - q_y)\ell) \\ &-f_+\left(\left(\frac{q_x + q_y}{\tan\alpha} + q_z\right)h\right)\exp(-i(q_x + q_y)\ell) \\ &-f_-\left(\left(\frac{q_x + q_y}{\tan\alpha} - q_z\right)h\right)\exp(+i(q_x + q_y)\ell)\Big\}, \end{aligned}$$

$$V = H\Big[L^2 - \frac{2LH}{\tan\alpha} + \frac{4}{3}\frac{H^2}{\tan^2\alpha}\Big].$$

$$S = L^2.$$

$$V = \frac{1}{6}L^3\tan\alpha\left[1 - \left(1 - \frac{2H}{L\tan\alpha}\right)^3\right],,$$

$$S = L^2.$$

Examples

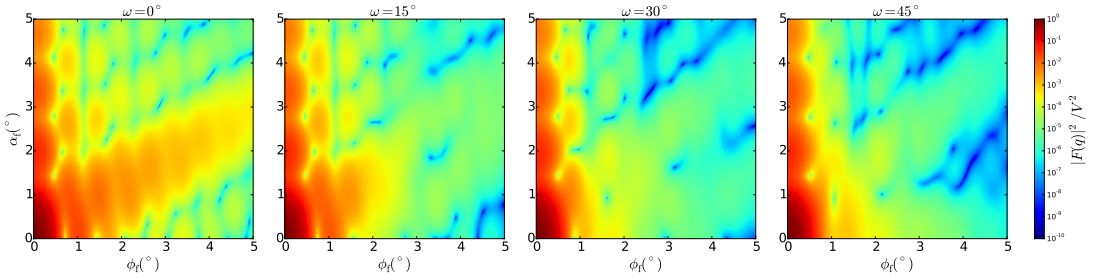

Figure B.28: Normalized intensity $|F|^2/V^2$, computed with $L = 10$ nm, $H = 4.2$ nm and $\alpha = 60°$, for four different angles ω of rotation around the z axis.

References

Corresponds to *Pyramid* form factor of `IsGISAXS` [7, Eq. 2.31] [8, Eq. 221], with different parametrization $L = 2R_{\texttt{IsGISXAXS}}$, with correction of a sign error, and with a more compact form of $F(\boldsymbol{q})$.

B.14 Ripple1 (sinusoidal)

Real-space geometry

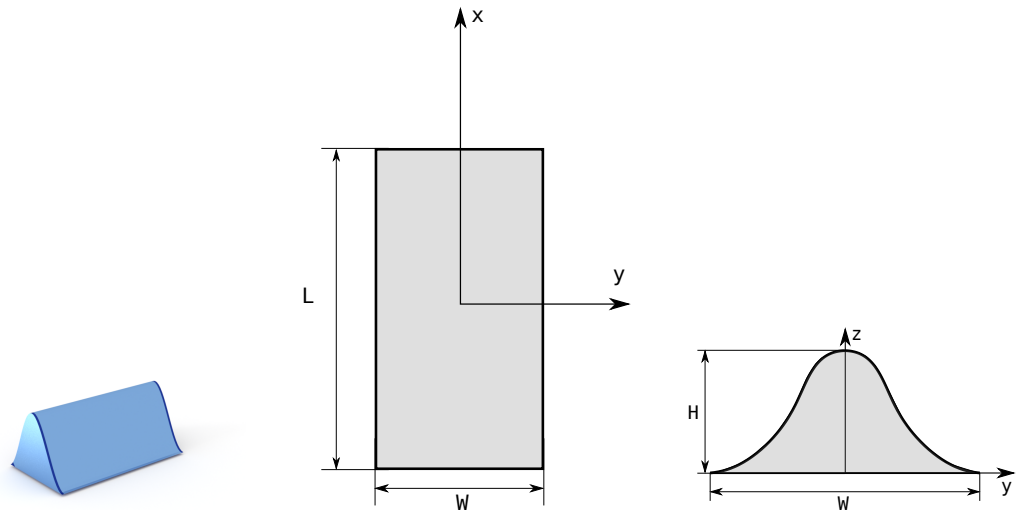

Perspective Top view Side view

Figure B.29: An infinite ripple with a sinusoidal profile.

Syntax and parameters

```
FormFactorRipple1(length, width, height)
```

with the parameters

- `length`, L,
- `width`, W,
- `height`, H.

Form factor etc

$$F = L \cdot \frac{W}{\pi} \cdot \operatorname{sinc}\left(\frac{q_x L}{2}\right) \times \int_0^H \mathrm{d}z \, \arccos\left(\frac{2z}{H} - 1\right) \operatorname{sinc}\left[\frac{q_y W}{2\pi} \arccos\left(\frac{2z}{H} - 1\right)\right] \exp\left(iq_z z\right),$$

$$V = \frac{LWH}{2},$$

$$S = LW.$$

Examples

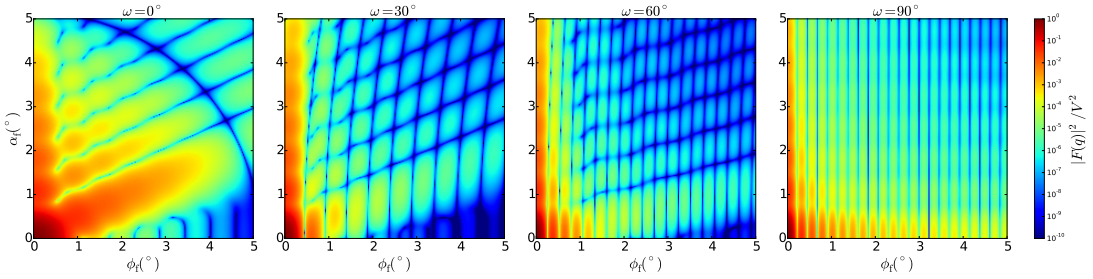

Figure B.30: Normalized intensity $|F|^2/V^2$, computed with $L = 25$ nm, $W = 10$ nm and $H = 8$ nm, for four different angles ω of rotation around the z axis.

References

Agrees with the *Ripple1* form factor of `FitGISAXS` [14].

B.15 Ripple2 (saw-tooth)

Real-space geometry

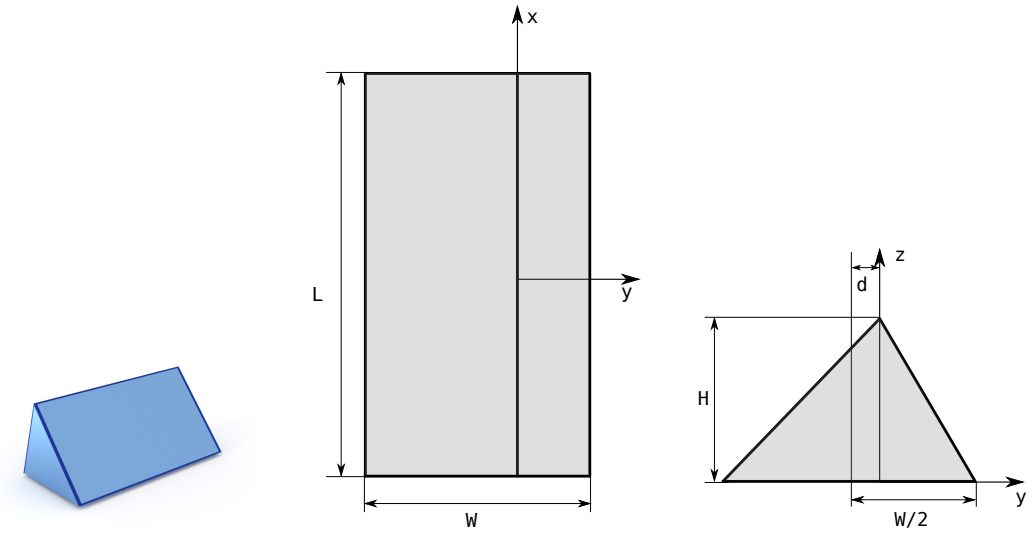

Perspective Top view Side view

Figure B.31: An infinite ripple with an asymmetric saw-tooth profile.

Syntax and parameters

```
FormFactorRipple2(length, width, height, asymmetry)
```

with the parameters

- `length`, L,
- `width`, W,
- `height`, H.
- `asymmetry`, d.

They must fulfill

$$|d| \leq W/2.$$

Form factor etc

$$F = LW \operatorname{sinc}\left(\frac{q_x L}{2}\right) \times \int_0^H \mathrm{d}z \left(1 - \frac{z}{H}\right) \operatorname{sinc}\left[\frac{q_y W}{2}\left(1 - \frac{z}{H}\right)\right] \exp\left\{i\left[q_z z - q_y d\left(1 - \frac{z}{H}\right)\right]\right\}$$

$$V = \frac{LWH}{2},$$
$$S = LW.$$

Examples

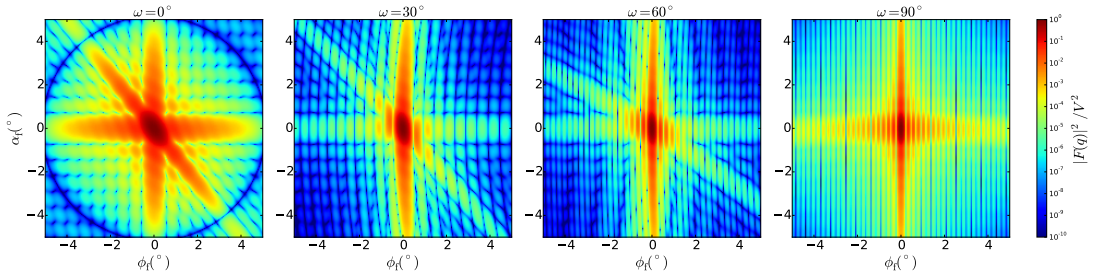

Figure B.32: Normalized intensity $|F|^2/V^2$, computed with $L = 25$ nm, $W = 10$ nm, $H = 8$ nm, and $d = 5$ nm, for four different angles ω of rotation around the z axis. The low symmetry requires other angular ranges than used in most other figures.

References

Agrees with the *Ripple2* form factor of `FitGISAXS` [14].

B.16 Tetrahedron

Real-space geometry

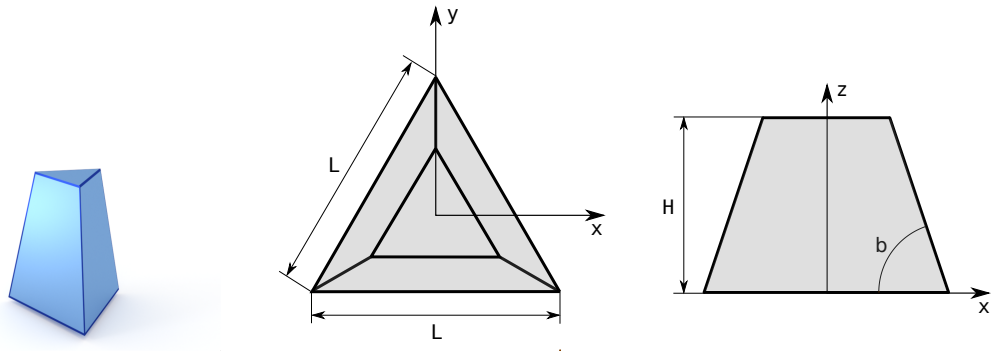

Perspective Top view Side view

Figure B.33: A truncated tetrahedron.

Syntax and parameters

```
FormFactorTetrahedron(length, height, alpha)
```

with the parameters

- `length` of one edge of the equilateral triangular base, L,
- `height`, H,
- `alpha`, angle between the base and a side face, α.

They must fulfill

$$H \leq \frac{\tan\alpha}{2\sqrt{3}} L.$$

Note that the orthographic projection does not show α, but the angle β between the base and a side edge. They are related through $\tan\alpha = 2\tan\beta$.

Form factor etc

Notation:

$$q_1 := \frac{1}{2}\left[\frac{q_x\sqrt{3} - q_y}{\tan\alpha} - q_z\right], \quad q_2 := \frac{1}{2}\left[\frac{q_x\sqrt{3} + q_y}{\tan\alpha} + q_z\right], \quad q_3 := \frac{q_y}{\tan\alpha} - \frac{q_z}{2}, \quad D := \frac{L\tan\alpha}{\sqrt{3}} - H.$$

Results:

$$F = \frac{\sqrt{3}H}{q_x(q_x^2 - 3q_y^2)} \exp\left(i\frac{q_z L\tan(\alpha)}{2\sqrt{3}}\right) \times$$
$$\Big\{2q_x \exp(iq_3 D)\,\mathrm{sinc}(q_3 H) - (q_x + \sqrt{3}q_y)\exp(iq_1 D)\,\mathrm{sinc}(q_1 H)$$
$$- (q_x - \sqrt{3}q_y)\exp(-iq_2 D)\,\mathrm{sinc}(q_2 H)\Big\},$$

$$V = \frac{\tan(\alpha) L^3}{24} \left[1 - \left(1 - \frac{2\sqrt{3} H}{L \tan(\alpha)} \right)^3 \right],$$

$$S = \frac{\sqrt{3}}{4} L^2.$$

Examples

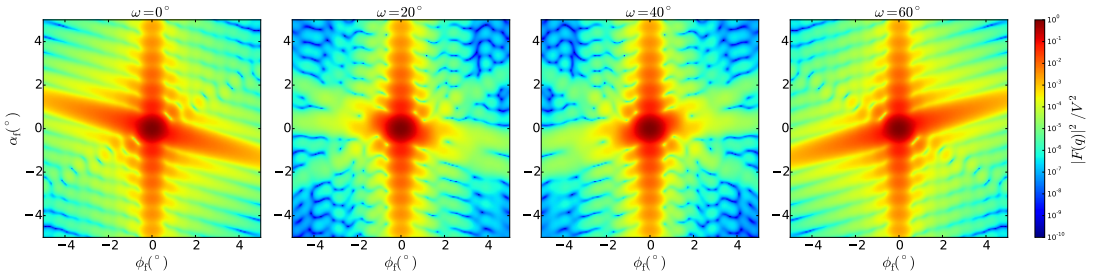

Figure B.34: Normalized intensity $|F|^2/V^2$, computed with $L = 12$ nm, $H = 8$ nm, and $\alpha = 75°$, for four different angles ω of rotation around the z axis. The low symmetry requires other angular ranges than used in most other figures.

References

Agrees with the *Tetrahedron* form factor of `IsGISAXS` [7, Eq. 2.30] [8, Eq. 220]. In `FitGISAXS` correctly called *Truncated tetrahedron* [14].

B.17 TruncatedCube

Real-space geometry

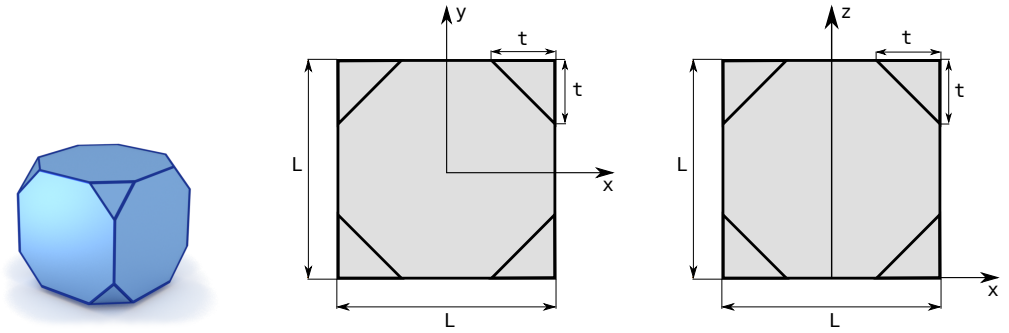

Perspective Top view Side view

Figure B.35: A cube whose eight vertices have been removed. The truncated part of each vertex is a trirectangular tetrahedron.

Syntax and parameters

```
FormFactorTruncatedCube(length, removed_length)
```

with the parameters

- `length` of the full cube, L,
- `removed_length`, side length of the trirectangular tetrahedron removed from the cube's vertices, t.

They must fulfill

$$t \leq L/2.$$

Form factor etc

Notation:
Besides the form factor $F_{\text{Box}}(\boldsymbol{q})$ of the full cube of side length L (Sect. B.2), we need the form factor of a trirectangular tetrahedrons as cut from the cube:

$$\begin{aligned} F_{\text{vertex}_1}(q_x, q_y, q_z, L, t) = \frac{t}{q_z} \exp\left(i\frac{q_x(L-t)+q_y L}{2}\right) \\ \times\Big\{\frac{1}{q_y}\operatorname{sinc}\left(\frac{q_x t}{2}\right) - \frac{q_z}{q_y(q_y+q_z)}\exp\left(i\frac{q_y t}{2}\right)\operatorname{sinc}\left(\frac{(q_x-q_y)t}{2}\right) \\ - \frac{1}{q_y+q_z}\exp\left(i\frac{q_z t}{2}\right)\operatorname{sinc}\left(\frac{(q_x+q_z)t}{2}\right)\Big\} \end{aligned}$$

Thanks to symmetry (see the following figure, which shows the vertices V_i for $i = 1, \ldots, 8$), the form factors of other seven tetrahedrons cut from the cube can be computed as follows (note that the origin is taken as usual at the centre of the bottom face of the cube):

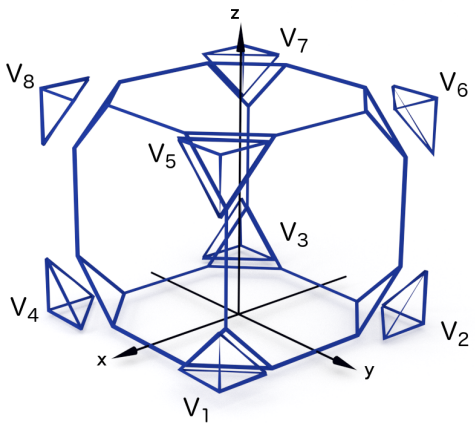

$$
\begin{aligned}
F_{\text{vertex}_2}(q_x, q_y, q_z, L, t) &= F_{\text{vertex}_1}(q_y, -q_x, q_z, L, t) \\
F_{\text{vertex}_3}(q_x, q_y, q_z, L, t) &= F_{\text{vertex}_1}(-q_x, -q_y, q_z, L, t) \\
F_{\text{vertex}_4}(q_x, q_y, q_z, L, t) &= F_{\text{vertex}_1}(-q_y, q_x, q_z, L, t) \\
F_{\text{vertex}_5}(q_x, q_y, q_z, L, t) &= \exp(iq_zL) F_{\text{vertex}_1}(q_x, q_y, -q_z, L, t) \\
F_{\text{vertex}_6}(q_x, q_y, q_z, L, t) &= \exp(iq_zL) F_{\text{vertex}_1}(q_y, -q_x, -q_z, L, t) \\
F_{\text{vertex}_7}(q_x, q_y, q_z, L, t) &= \exp(iq_zL) F_{\text{vertex}_1}(-q_x, -q_y, -q_z, L, t) \\
F_{\text{vertex}_8}(q_x, q_y, q_z, L, t) &= \exp(iq_zL) F_{\text{vertex}_1}(-q_y, q_x, -q_z, L, t)
\end{aligned}
$$

Result:

$$
F = F_{\text{Box}}(q_x, q_y, q_z, L, L, L) - \sum_{i=1}^{8} F_{\text{vertex}_i}(q_x, q_y, q_z, L, t)
$$

$$
V = L^3 - \frac{4}{3}t^3,
$$

$$
S = L^2.
$$

Examples

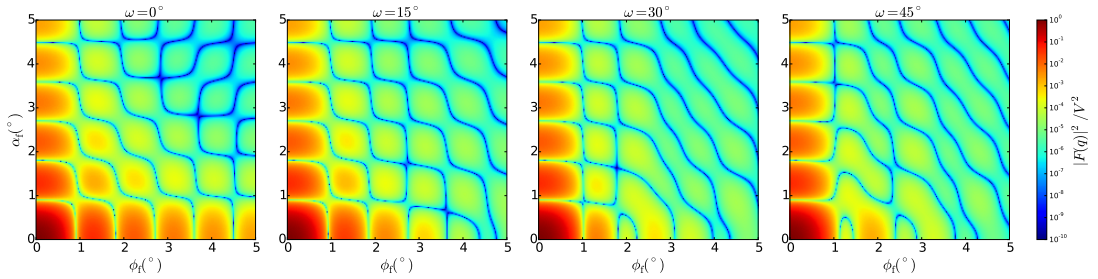

Figure B.36: Normalized intensity $|F|^2/V^2$, computed with $L = 25$ nm, $W = 10$ nm, $H = 8$ nm, and $d = 5$ nm, for four different angles ω of rotation around the z axis.

References

[15]

Page intentionally left blank

B.18 TruncatedSphere

Real-space geometry

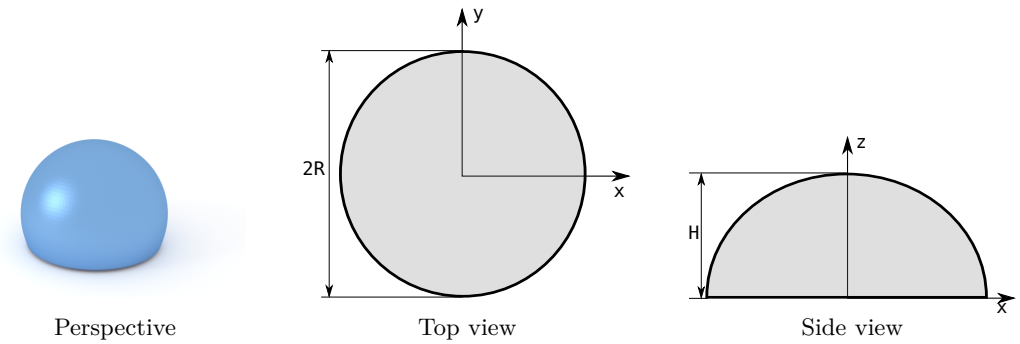

Figure B.37: A truncated sphere.

Syntax and parameters

```
FormFactorTruncatedSphere(radius, height)
```

with the parameters

- `radius`, R,
- `height`, H.

They must fulfill

$$0 < H \leq 2R.$$

Form factor etc

Notation:

$$q_{\parallel} := \sqrt{q_x^2 + q_y^2}, \quad R_z := \sqrt{R^2 - z^2}.$$

Results:

$$F = 2\pi \exp[iq_z(H-R)] \int_{R-H}^{R} \mathrm{d}z\, R_z^2 \frac{J_1(q_{\parallel} R_z)}{q_{\parallel} R_z} \exp(iq_z z) dz,$$

$$V = \pi R^3 \left[\frac{2}{3} + \frac{H-R}{R} - \frac{1}{3} \left(\frac{H-R}{R} \right)^3 \right],$$

$$S = \begin{cases} \pi R^2, & H \geq R \\ \pi \left(2RH - H^2\right), & H < R \end{cases}.$$

Example

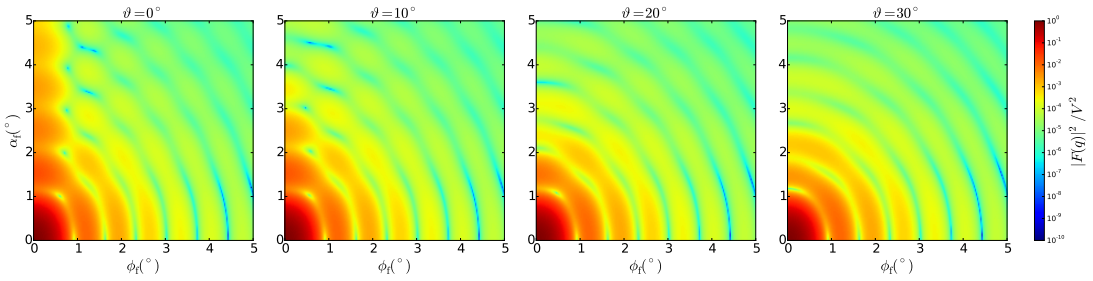

Figure B.38: Normalized intensity $|F|^2/V^2$, computed with $R = 4.2$ nm and $H = 6.1$ nm, for four different tilt angles ϑ (rotation around the y axis).

References

Agrees with the `IsGISAXS` form factor *Sphere* [7, Eq. 2.33] or *Truncated sphere* [8, Eq. 228].

B.19 TruncatedSpheroid

Real-space geometry

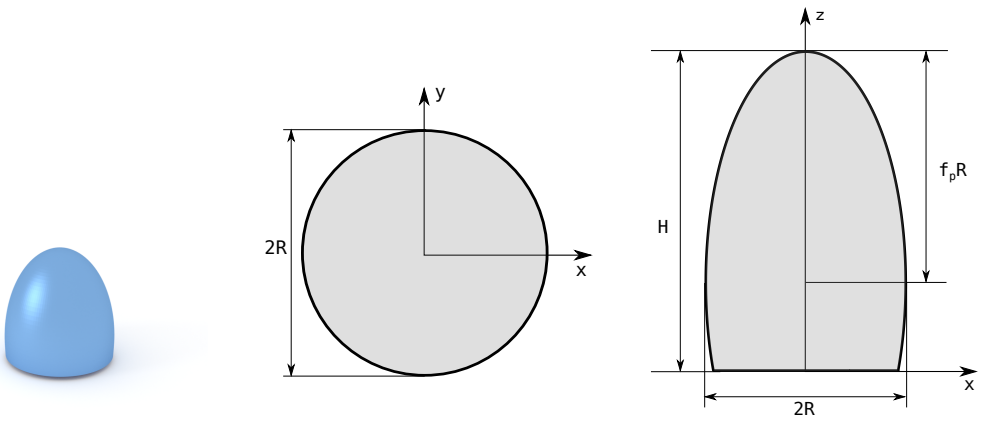

Perspective Top view Side view

Figure B.39: A vertically oriented, horizontally truncated spheroid.

Syntax and parameters

```
FormFactorTruncatedSpheroid(radius, height, height_flattening)
```

with the parameters

- `radius`, R,
- `height`, H.
- `height_flattening`, f_p.

They must fulfill

$$0 < \frac{H}{R} \leq 2f_p.$$

Form factor etc

Notation:

$$q_\parallel := \sqrt{q_x^2 + q_y^2}, \quad R_z := \sqrt{R^2 - z^2/f_p^2}.$$

Results:

$$F = 2\pi \exp[iq_z(H - f_pR)] \int_{f_pR-H}^{f_pR} \mathrm{d}z\, R_z^2 \frac{J_1(q_\parallel R_z)}{q_\parallel R_z} \exp(iq_z z)$$

$$V = \frac{\pi R H^2}{f_p}\Big(1 - \frac{H}{3f_pR}\Big),$$

$$S = \begin{cases} \pi R^2, & H \geq f_p R \\ \pi \left(\dfrac{2RH}{f_p} - \dfrac{H^2}{f_p^2} \right), & H < R \end{cases} .$$

Example

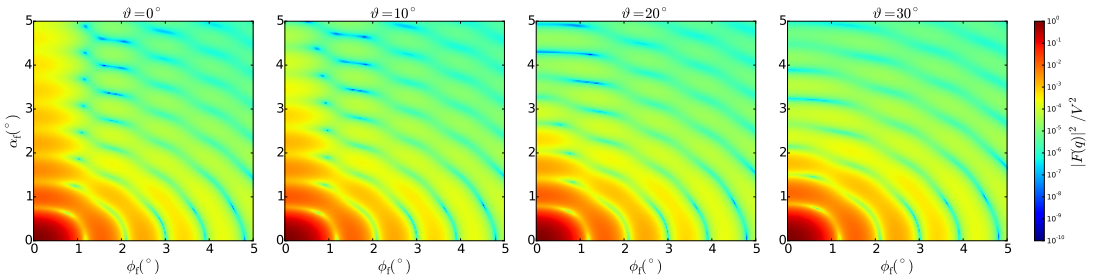

Figure B.40: Normalized intensity $|F|^2/V^2$, computed with $R = 3.3$ nm, $H = 9.8$ nm, and $f_p = 1.8$, for four different tilt angles ϑ (rotation around the y axis).

References

Agrees with the `IsGISAXS` form factor *Sphere* [7, Eq. 2.33] or *TruncatedSpheroid* [8, Eq. 228].

Bibliography

[1] MARIA. Magnetic reflectometer with high incident angle. http://www.mlz-garching.de/maria.

[2] NREX. Neutron reflectometer with X-ray option. http://www.mlz-garching.de/nrex.

[3] REFSANS. Horizontal TOF Reflectometer with GISANS option. http://www.mlz-garching.de/refsans.

[4] High Data Rate Processing and Analysis Initiative (HDRI) of the Helmholtz Association of German research centres. http://www.pni-hdri.de.

[5] SINE2020: world-class Science and Innovation with Neutrons in Europe in 2020. http://cordis.europa.eu/news/rcn/124015_en.html.

[6] R. Lazzari, J. Appl. Cryst. **35**, 406 (2002).

[7] R. Lazzari, IsGISAXS manual, version 2.6, http://www.insp.jussieu.fr/oxydes/IsGISAXS/figures/doc/manual.html [as per May 2015].

[8] G. Renaud, R. Lazzari and F. Leroy, Surface Science Reports **64**, 255 (2009).

[9] V. P. Sears, *Neutron Optics*, Oxford University Press: Oxford (1989).

[10] M. Lax, Rev. Mod. Phys. **23**, 287 (1951).

[11] M. Born and E. Wolf, *Principles of Optics*, Cambridge University Press: Cambridge (^{7}1999).

[12] E. Hecht, *Optics*, Addison Wesley: San Francisco (^{4}2002).

[13] M. Abramowitz and I. Stegun, *Handbook of Mathematical Functions*, National Bureau of Standards (1964).

[14] D. Babonneau, FitGISAXS manual, version May 2013, http://www.pprime.fr/sites/default/files/pictures/d1/FINANO/FitGISAXS_130531.zip [as per May 2015].

[15] R. W. Hendricks, J. Schelten and W. Schmatz, Philos. Mag. **30**, 819 (1974).

List of Symbols

$:=$	Defines what is on the left, page 7
$=:$	Defines what is on the right, page 7
$\equiv$	Equal as result of a definition, page 7
$\simeq$	Asymptotically equal: equal in an implied limit, page 7
$\doteq$	Equal up to first order of a power-law expansion, hence a special case of asymptotic equality, page 7
$\langle ... \mid ... \mid ... \rangle$	Matrix element, defined as a volume integral, page 14
$\pm$	Upward (+) or downward (−) propagating, page 19
α_{f}	Glancing angle of the detected beam, page 17
α_{i}	Glancing angle of the incident beam, page 17
β	Imaginary part of the refractive index, page 19
δ	Small parameter in the refractive index $n = 1 - \delta + i\beta$, page 19
$\rho_s(\boldsymbol{r})$	Scattering length density, page 11
σ	Scattering or absorption cross section, page 15
$\phi(z)$	z-dependent factor of $\psi(\boldsymbol{r})$, page 17
ϕ_{f}	Angle between the detected beam, projected into the sample plane, and the x axis, page 17
ϕ_{i}	Angle between the incident beam, projected into the sample plane, and the x axis, page 17
$\chi(\boldsymbol{q})$	Fourier transform of the perturbation potential $\chi(\boldsymbol{r})$, page 14
$\chi(\boldsymbol{r})$	Perturbative potential, for neutrons equal to the scattering-length density ρ_s, page 12
$\chi_l(\boldsymbol{q})$	Fourier transform of the perturbation potential $\chi(\boldsymbol{r})$, evaluated in one sample layer, page 23

$\psi(\boldsymbol{r})$	Stationary wavefunction, page 10
$\psi(\boldsymbol{r}, t)$	Microscopic neutron wavefunction, page 10
$\psi(\boldsymbol{r}, t)$	Coherent wavefunction, page 11
$\psi_{\mathrm{f}}(\boldsymbol{r})$	Plane wave propagating from the sample towards the detector, page 14
$\psi_{\mathrm{i}}(\boldsymbol{r})$	Incident wavefunction, page 12
$\psi_{\mathrm{s}}(\boldsymbol{r})$	Scattered wavefunction, page 13
$\psi_{\mathrm{s,far}}(\boldsymbol{r})$	Far-field approximation to the scattered wavefunction $\psi_{\mathrm{s}}(\boldsymbol{r})$, page 14
$\psi^{\pm}(\boldsymbol{r})$	Upward (+) or downward (−) propagating component of $\psi(\boldsymbol{r})$, page 19
ω	Frequency of incident radiation, page 10
Ω	Solid angle, page 15
$A^{\pm}_{wl}$	Amplitude of the plane wave $\phi^{\pm}_{wl}(\boldsymbol{r})$, page 22
$B(\boldsymbol{r}, \boldsymbol{r}')$	Green function, adjoint of G, page 18
f	Subscript "final", for outgoing waves scattered into the direction of the detector, page 14
$G(\boldsymbol{r}, \boldsymbol{r}')$	Green function, page 13
$G_{\mathrm{far}}(\boldsymbol{r}, \boldsymbol{r}')$	Far-field approximation to the Green function $G(\boldsymbol{r}, \boldsymbol{r}')$, page 14
i	Subscript "incident", page 12
J_1	Bessel function of first kind and first order, page 32
$\boldsymbol{J}(\boldsymbol{r})$	Probability flux, page 15
$k_{\perp}$	Component of $\boldsymbol{k}$ along the sample normal, page 17
$\boldsymbol{k}$	wavevector, page 14
$\boldsymbol{k}_{\parallel}$	Projection of $\boldsymbol{k}$ onto the sample plane, page 17
$\boldsymbol{k}^{\pm}_{wl}$	wavevector of the plane wave $\psi^{\pm}_{wl}(\boldsymbol{r})$, page 21
K	Vacuum wavenumber, corresponding to the frequency ω, page 11
l	Index of layer in multilayer sample, page 21
m	Neutron mass, page 11
$n(\boldsymbol{r})$	Refractive index, page 11
$\overline{n^2}(z)$	Refractive index, horizontally averaged, page 16

$\boldsymbol{q}$	Scattering vector, page 14
$\boldsymbol{r}$	Position, page 10
$\boldsymbol{r}_{\mathrm{D}}$	Position of the detector, page 18
R_{wl}	Partial amplitude of $\psi_w(\boldsymbol{r})$ in layer l in upward (reflection) direction, also denoted A^+_{wl}, page 22
s	Subscript "scattered", page 13
sinc	Cardinal sine, $\mathrm{sinc}(x) \coloneqq \sin(x)/x$, page 7
S	Maximum horizontal section of embedded particle, page 32
t	Time, page 10
T_{wl}	Partial amplitude of $\psi_w(\boldsymbol{r})$ in layer l in downward (transmission) direction, also denoted A^-_{wl}, page 22
$v(\boldsymbol{r})$	Macrosopic optical potential, page 11
$V(\boldsymbol{r})$	Microscopic optical potential, page 11
w	An index that can take the values i (incident) or f (final), page 19
x	Horizontal coordinate, usually chosen along the incoming beam projection, page 17
y	Horizontal oordinate, chosen normal to z and x, page 17
z_l	Vertical coordinate at the top of layer l (at the bottom for $l = 0$), page 22
z	Vertical coordinate, along the sample normal, page 16
$\hat{\boldsymbol{z}}$	Unit vector along the sample normal, page 21

Index

Absorption, 19–20
Anisotropic pyramid (form factor), 34
API, *see* Application programming interface
Application programming interface, 9

Born approximation, 12–13
Box (form factor), 36
Bragg scattering
  by atomic lattices, 11
Bug reports, 6

C++, 9
Citation, 5
Coherent forward scattering, 11
Coherent wavefunction, 11
Cone (form factor)
  circular, 38
  hexagonal (Cone6), 40
Continuum approximation
  neutron propagation, 11
Conventions, *see* Sign convention, *see* Horizontal and Vertical
Coordinate system, 14
Cross section, 15
Cube (form factor)
  facetted, 66
Cuboctahedron (form factor), 42
Cuboid (form factor), 36
Cylinder (form factor), 44
  ellipsoidal, 46

Detector
  mapping the cross section, 6
  transmission geometry, 25
Dissipation, 26
Distorted-wave Born approximation, 5, 18–19
  multilayer, 22
Download, 8

DWBA, *see* Distorted-wave Born approximation

Ellipsoid (form factor)
  truncated, 50
Ellipsoidal cylinder (form factor), 46
Evanescent wave, 26

Facetted cube (form factor), 66
Far-field approximation, 13–14, 18
Fermi's pseudopotential, 11
Flux
  incident and scattered, 15
Form factor, 73
`FormFactorAnisoPyramid`, 34
`FormFactorBox`, 36
`FormFactorCone`, 38
`FormFactorCone6`, 40
`FormFactorCuboctahedron`, 42
`FormFactorCylinder`, 44
`FormFactorEllipsoidalCylinder`, 46
`FormFactorFullSphere`, 48
`FormFactorFullSpheroid`, 52
`FormFactorHemiEllipsoid`, 50
`FormFactorPrism3`, 54
`FormFactorPrism6`, 56
`FormFactorPyramid`, 58
`FormFactorRipple1`, 60
`FormFactorRipple2`, 62
`FormFactorTetrahedron`, 64
`FormFactorTruncatedCube`, 66
`FormFactorTruncatedSphere`, 70
`FormFactorTruncatedSpheroid`, 72
Forum, 9
Fraunhofer approximation, 13
Fresnel coefficients, 18, 23
Full sphere (form factor), 48
Full spheroid (form factor), 52

Glancing angle, 16

Green function
homogeneous material, 13, 14
reciprocity, 28
vertically structured material, 18

Helmholtz equation, 12
Hemi ellipsoid (form factor), 50
Hole, 27
Horizontal plane, 16
Huygens' principle, 11

Inclusion, 27
Index of refraction, *see* Refractive index
Installation, 8
`IsGISAXS`, 6
Island, 27

Layer
coordinate, 22
index, 21, 22
transfer matrix, 24
Layer structures, *see* Multilayer
Lazzari, Rémi, 6
Linux, 8
Lippmann-Schwinger equation, 13

MacOS, 8
Mesoparticles, *see* Particles
Microsoft Windows, 8
Momentum transfer, *see* Scattering vector
Multilayer, 21–26
coordinates, 22
numbering, 21, 22
transfer matrix, 24

Nanoparticles, *see* Particles
Neutrons
polarization, 6
wave propagation, 10–12
Newsletter, 9

Operating system, 8
Optical potential
Fourier transform, 14
macroscopic, 11
nuclear (microscopic), 11

Particle assemblies, 6, 27
Perturbation, 12
Phase integral method, *see* WKB method
Platform (operating system), 8
Polarized neutron
propagation and magnetic scattering, 6
Potential, *see* Optical potential, *see* Perturbation
Prism (form factor)
hexagonal (Prism6), 56
reactangular (Box), 36
triangular (Prism3), 54
Pyramid (form factor)
hexagonal (Cone6), 40
rectangular (AnisoPyramid), 34
square, 58
Python, 9

Quadrature, 32

Reciprocity, 18, 28–29
Reflection, 16, *see also* Fresnel coefficients
Refraction, 16
Snell's law, 22
Refractive index, 11
graded, 18
sign convention, 11, 19
Registration, 9
Ripple (form factor)
saw-tooth (Ripple2), 62
sinusoidal (Ripple1), 60
Roughness, 6

Sample normal, 16
Sample plane, 16
SAS, *see* Small-angle scattering
Saw-tooth ripple (form factor), 62
Scattering length density, 11
Scattering vector, 14
Schrödinger equation
macroscopic, 11
microscopic, 10
Semiclassical approximation, *see* WKB method
Shape transform, 73
Sign convention, 20
scattering vector, 14
wave propagation, 10
Sinusoidal ripple (form factor), 60
Small-angle scattering, 10–12
Snell's law, 22
Sphere (form factor), 48
truncated, 70
Spheroid (form factor), 52
truncated, 72

Tetrahedron (form factor), 64
Total reflection, 26
Transfer matrix, 24
Transition matrix, 14
Transmission, *see* Fresnel coefficients
Transmission geometry, 25
Truncated cone (form factor), 38
Truncated ellipsoid (form factor), 50
Truncated pyramid (form factor)
    hexagonal (Cone6), 40
    rectangular (AnisoPyramid), 34
    square, 58
Truncated sphere (form factor), 70
Truncated spheroid (form factor), 72
Truncated tetrahedron (form factor), 64
Tunneling, 26

Tutorials, 9

Vertical direction, 16

Wave propagation, *see also* Sign convention
    coherent, 11
    neutrons, 10–12
    neutrons, polarized, 6
    X-rays, 6
Wavevector
    complex, 26
Windows, *see* Microsoft Windows
WKB method, 18

X-rays
    propagation and scattering, 6